



## A multistep approach for joint modeling of surface wave dispersion and teleseismic receiver functions: Implications for lithospheric structure of the Arabian Peninsula

H. Tkalčić,<sup>1,2</sup> M. E. Pasyanos,<sup>1</sup> A. J. Rodgers,<sup>1</sup> R. Gök,<sup>1</sup> W. R. Walter,<sup>1</sup> and A. Al-Amri<sup>3</sup>

Received 29 October 2005; revised 7 July 2006; accepted 15 August 2006; published 29 November 2006.

[1] We present a multiple step procedure for joint modeling of surface wave group velocity dispersion curves and teleseismic receiver functions for lithospheric velocity structure. The method relies on an initial grid search for a simple crustal structure, followed by a formal iterative inversion, an additional grid search for shear wave velocity in the mantle, and finally, forward modeling of transverse isotropy to resolve Love-Rayleigh surface wave dispersion discrepancy. It considers longer-period surface wave group velocity (SWGV) dispersion, allowing for the resolution of deeper structure compared to previous joint inversions. The grid search for simple crustal structure is facilitated using a library of precomputed receiver functions and SWGV dispersion curves. The iterative inversion improves fit to the data by increasing the number of layers in the crust when necessary. In order to fit the SWGV for periods greater than about 50 s, we perform a grid search over mantle velocities including the mantle lid and low-velocity zone, keeping the crustal structure fixed to the values from the previous step. In some cases a clear Love-Rayleigh discrepancy prevents a simultaneous fit of the group velocities with an isotropic model. The Love-Rayleigh discrepancy can be resolved by allowing shear wave transverse isotropy with a vertical symmetry axis ( $v_{SH} - v_{SV}$  differences) in the uppermost mantle. The method is applied to 10 stations in the Arabian Peninsula sampling various tectonic environments including active continental rifting and stable regions. The resulting shear velocity models confirm rapid crustal thinning of the Arabian Shield toward the Red Sea; however, we do not find strong evidence for crustal thickening toward the Arabian Platform. Our results suggest that the mantle lithosphere thickness varies regionally but that the mantle shear velocities beneath the Arabian Shield and Red Sea coast are generally anomalously low. Furthermore, our results indicate the presence of strong polarization anisotropy (up to about 10%) in the lithospheric upper mantle, in the vicinity of, as well as farther away from, the Red Sea. Our modeling yields  $v_{SV} > v_{SH}$  in the southwestern part of the Arabian Peninsula, consistent with vertical flow, and  $v_{SH} > v_{SV}$  in the northwestern part of the Arabian Peninsula and the continental interior, consistent with horizontal flow, indicating that the mantle flow pattern is not uniform along the axis of the Red Sea.

**Citation:** Tkalčić, H., M. E. Pasyanos, A. J. Rodgers, R. Gök, W. R. Walter, and A. Al-Amri (2006), A multistep approach for joint modeling of surface wave dispersion and teleseismic receiver functions: Implications for lithospheric structure of the Arabian Peninsula, *J. Geophys. Res.*, *111*, B11311, doi:10.1029/2005JB004130.

### 1. Introduction

[2] Since the beginning of broadband digital seismometry in the late 1970s, teleseismic receiver functions (RFs) have been used to estimate regional crustal structure [e.g.,

Langston, 1979; Owens, 1987; Owens *et al.*, 1987; Ammon *et al.*, 1990; Ammon, 1991]. This widely applied method deconvolves the vertical component P wave from the radial component to isolate the shear wave response of the crust and upper mantle beneath the recording station. RFs are very sensitive to changes in seismic velocities (i.e., discontinuities), however, are only weakly sensitive to absolute velocities. Methods to model crustal structure with RFs have relied on formal inversion [e.g., Ligorría and Ammon, 1999; Ammon *et al.*, 1990], or grid search [e.g., Sandvol *et al.*, 1998a], and similarly, genetic algorithm inversion of receiver functions [Shibutani *et al.*, 1996], based on the

<sup>1</sup>Atmospheric, Earth and Energy Sciences Department, Lawrence Livermore National Laboratory, Livermore, California, USA.

<sup>2</sup>Now at Multimax, Inc., Emeryville, California, USA.

<sup>3</sup>Geology Department, King Saud University, Riyadh, Saudi Arabia.

algorithm developed by *Sambridge and Drijkoningen* [1992]. There were several studies recently, however, in which RFs were jointly inverted with surface waves (SW) dispersion for crustal structure [e.g., *Özalaybey et al.*, 1997; *Du and Foulger*, 1999; *Julià et al.*, 2000]. These methods have the advantage of improved sensitivity to absolute velocities compared to RFs alone. In this paper we extend the method of *Julià et al.* [2000] by combining grid search, formal inversion and forward methods and by considering broadband long-period surface wave group velocities and mantle anisotropy. The method we are proposing is conceptually similar to the method by *Julià et al.* [2000] only in that it uses the same type of data and that it has the same goal, i.e., we seek seismic velocity depth profiles in the region of interest, which can explain the observed seismic data. However, we include long-period dispersion in the modeling and introduce an additional grid search for the structure in the mantle. Furthermore, we address the Love-Rayleigh wave dispersion discrepancy by additional forward modeling for the transverse isotropy. Above all, the final solution dependence on the starting model, which we believe is the largest and the most serious shortcoming of the existing linearized inversion schemes, is addressed with introducing the grid search step in the early stage of the procedure. In summary, the proposed method represents an improvement in existing methods for the following reasons:

[3] 1. The first grid search finds the optimal starting model for the linearized inversion and minimizes possible bias due to poor starting models. This results in a more time-consuming, but fundamentally more accurate modeling. The grid search allows users to study even those areas for which prior geological and geophysical a priori constraints do not exist.

[4] 2. The consideration of long-period surface wave group velocity (SWGv) data allows for deeper structure to be estimated but must result in crustal structure consistent with shorter-period SWGV and RF data.

[5] 3. The consideration of the lithospheric thickness and Love-Rayleigh discrepancy is required when considering the longer-period SWGV data (in most cases) and our additional grid search and forward modeling allow for a very general representation of mantle velocities.

[6] Some of the main shortcomings of receiver function analysis, such as possible effects of heterogeneity, anisotropy, and dipping interfaces on RFs, as well as the assessment of uncertainties in recovered models, remain to be addressed better in the future. However, in the application of this method, the objective is to improve estimates of one-dimensional average crustal and mantle lithospheric shear velocity structure beneath the stations of an insufficiently studied region, the Arabian Peninsula. The resulting models are optimized given the assumption of a plane-layered transversely isotropic Earth.

[7] The Arabian Peninsula forms a single tectonic plate, the Arabian Plate (Figure 1). It is surrounded on all sides by active plate boundaries. Active tectonics of the region is dominated by the collision of the Arabian Plate with the Eurasian Plate along the Zagros and Bitlis Thrust systems, rifting and seafloor spreading in the Red Sea and Gulf of Aden. Strike-slip faulting occurs along the Gulf of Aqaba and Dead Sea Transform fault systems. Two large provinces associated with the presence or absence of sedimentary

cover define the large-scale geologic structure of the Arabian Peninsula. The Arabian Platform (eastern Arabia) is covered by sediments that thicken significantly toward the Persian Gulf. The Arabian Shield has no appreciable sedimentary cover with many outcrops. Volcanic activity is observed on the Arabian Shield. This is likely to be related to the opening of the Red Sea and mantle asthenospheric upwelling beneath western Arabia [e.g., *Camp and Roobol*, 1992].

[8] Previous studies of crustal and upper mantle structure of the Arabian Peninsula have reported differences between the structure of the Arabian Shield and the Arabian Platform. However, early investigations were limited by the paucity of available waveform data. Some of these studies relied on analog surface wave data [e.g., *Knopoff and Fouda*, 1975; *Mokhtar and Al-Saeed*, 1994; *Al-Amri*, 1999]. More recently, seismological studies of the Arabian shield relied on data recorded by the Saudi Arabian Portable Broadband Deployment [*Vernon et al.*, 1996; *Vernon and Berger*, 1998; *Mellors et al.*, 1999].

[9] Teleseismic RFs were calculated for numerous of stations in the Arabian Peninsula in several seismological studies. For example, *Sandvol et al.* [1998b] estimated the lithospheric structure of the Arabian Shield by modeling receiver function stacks obtained from teleseismic P waves. *Levin and Park* [2000] observed strong azimuthal variations of RFs at station RAYN (Ar Rayn, Saudi Arabia) and proposed a model of two anisotropic zones bounded, respectively, by the sharp Moho and the Hales discontinuity on the top. Furthermore, possible complex azimuthal anisotropy patterns exist based on limited shear wave splitting observations (such as *Levin et al.* [2006]). However, *Wolfe et al.* [1999] and, recently, *Hansen et al.* [2006] reported that shear wave splitting orientations are consistently slightly east of north at stations in Arabia and this tendency is remarkably stable across the Arabian Plate. These observations do not support a complex anisotropy and can be explained by a simple combination of plate motion and channelized flow along the Red Sea. *Julià et al.* [2003] presented receiver function results for the Arabian Shield, combining them with surface wave dispersion data to invert for the lithospheric structure. *Al-Damegh et al.* [2005] calculated RFs for the Arabian Plate from permanent broadband stations in Saudi Arabia [*Al-Amri and Al-Amri*, 1999] and Jordan [*Rodgers et al.*, 2003a].

[10] With a goal of improving structural estimates of the Eurasian lithosphere, Lawrence Livermore National Laboratory (LLNL) has collaborative projects with a number of institutions in the Middle East. LLNL participated in deploying broadband instruments HITJC and RUWJC in Jordan [*Rodgers et al.*, 2003a] and MEZE and HALE in UAE [*Rodgers et al.*, 2003b]. Recently, M. E. Pasyanos et al. (Seismic structure of Kuwait: A case study of improvements to structural estimates from the installation of a broadband station, submitted to *Geophysical Journal International*, 2005, hereinafter referred to as Pasyanos et al., submitted manuscript, 2005) employed SWGV dispersion and RFs from broadband waveform data at the station KBD to derive crustal structure of Kuwait. In this paper, using a newly developed multistep method, we extend previous efforts to determine crustal and lithospheric mantle structure under the stations of the Arabian Peninsula. We use an extended data

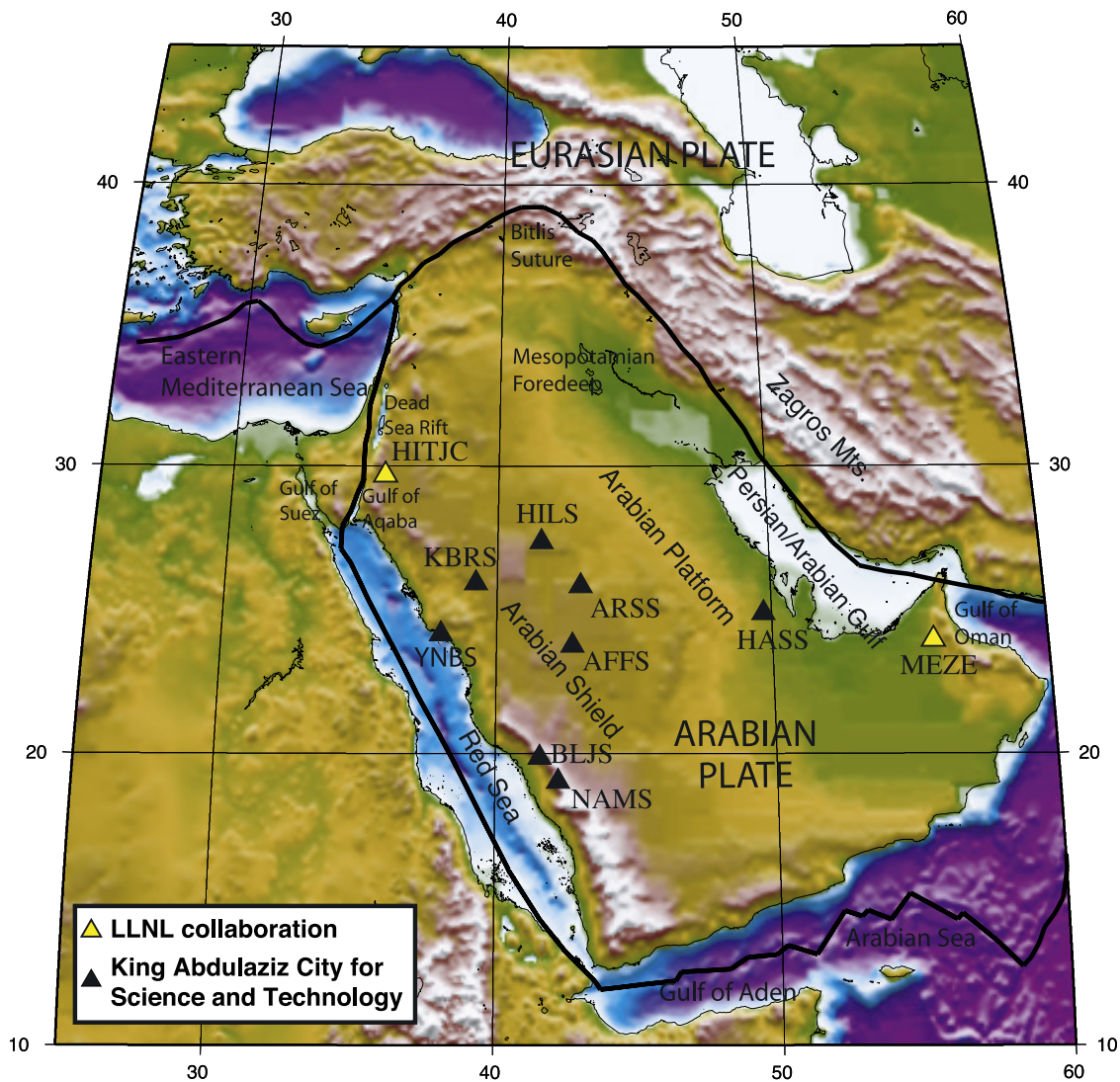


**Figure 1.** Regional map of the Arabian Peninsula. The triangles denote the locations of the stations used in this study. Also shown are plate boundaries (solid lines) and names of main tectonic and geographic features.

set from previously analyzed stations and several more stations that have meanwhile become available.

## 2. Data

### 2.1. Teleseismic Receiver Function Data

[11] We estimate teleseismic RFs from a significant number of high-quality waveform data. Unprocessed data for RF analysis consist of three-component broadband velocity seismograms for earthquakes with magnitudes  $m_b > 5.8$  and epicentral distances between  $30^\circ$  and  $90^\circ$ . Global earthquake distribution for station HILS in the middle part of the Arabian Peninsula is shown in Figure 2a. Most of the seismicity occurring at epicentral distances suitable to use for the receiver function method are confined in the western part of the Pacific Rim, from the Kuril Islands in the north to the Indonesia in the south.

[12] In order to produce radial receiver functions at each station, we used the time domain iterative deconvolution procedure described by *Ligorria and Ammon* [1999]. Prior to applying the deconvolution procedure, we cut traces at

5 s before and 30 s after the main P arrival. Resulting receiver functions from a number of earthquakes could be stacked and averaged for a range of back azimuths. However, averaging can result in reducing the amplitudes of some important features, especially at later times of the receiver function time series where signal from the crust is weak. Therefore special care is taken in selecting only mutually coherent waveforms, resulting from at least 10 or more earthquakes. We also checked how RFs vary at each station with azimuth and ray parameter of the incoming waves and found that this variation is not very significant. Surely, as previously observed for station RAYN [*Levin and Park*, 2000], there are some variations with azimuth in the RFs for the stations on the Arabian Peninsula. However, we estimated that RFs variation with back azimuth is less significant in the context of meeting our most important goals: (1) overall simultaneous fitting of RFs and surface wave dispersion at short periods, (2) explaining long-period surface wave dispersion, and (3) explaining Love-Rayleigh dispersion discrepancy. Although we considered eastern back azimuths, we found that the data from

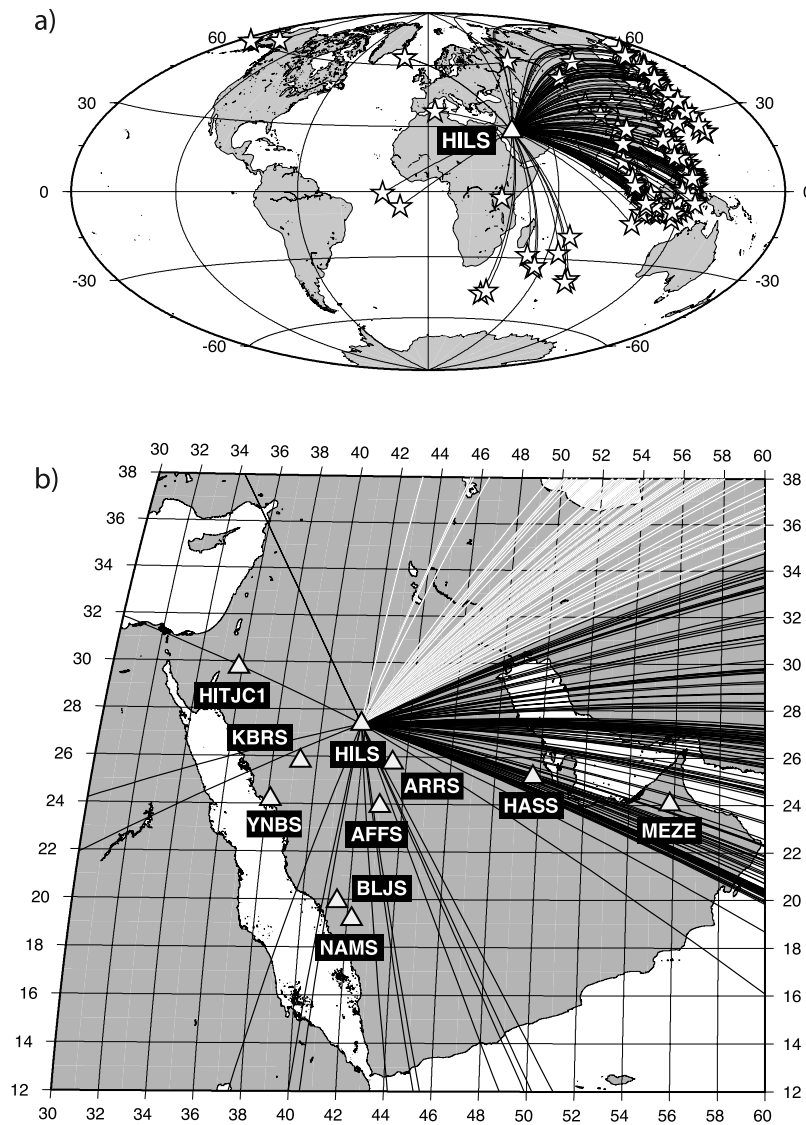


**Figure 2.** (a) Global distribution of events for which broadband waveform data were available at station HILS (events  $m_b \geq 5.2$  from January 2000 to November 2003). (b) A detail from Figure 2a, with highlighted ray paths used to obtain an averaged receiver function at station HILS shown in Figure 3.

northeastern back azimuths were of the best quality and therefore we used them for average receiver function estimates. As an example, we highlighted in Figure 2b the band of ray paths used to obtain an average receiver function at station HILS. In general, there is almost no difference among the RFs corresponding to the earthquakes from the Philippines and Indonesia back azimuths. Small difference is seen with respect to them for the RFs corresponding to the Kuril Islands/Japan earthquakes. Since we felt more confident with the quality and a larger number of RFs being mutually more coherent (better cross correlated with a larger number of other RFs) for the Kuril Islands earthquakes, we selected the corresponding RFs to obtain a representative RF for this station. Since the number of waveforms is quite large, we have the luxury of using only data from a relatively narrow subrange of available back azimuths at similar epicentral distances to increase the coherence.

[13] Small variations in the RFs for different back azimuths may be due to a range of effects like anisotropy and/or dipping layers. However, these differences are clearly quite small. The Ps Moho phase is generally identical for each back azimuth and slight differences arise at later times in the RF. These differences are not large enough to preclude accurate estimation of average structure near the station. In fact, the RFs from any back azimuths would produce the same average structure sought by the procedure.

[14] Figure 3a shows a bundle of receiver functions estimated from earthquakes highlighted in Figure 2b for station HILS, and the same for station HASS. A very coherent receiver function with common features corresponding to P to S conversions is visible after overlaying and plotting together all receiver functions. Some receiver functions in Figure 3a are noisy because the original records are noisy, and also because deconvolution is an unstable process. After visual examination and careful

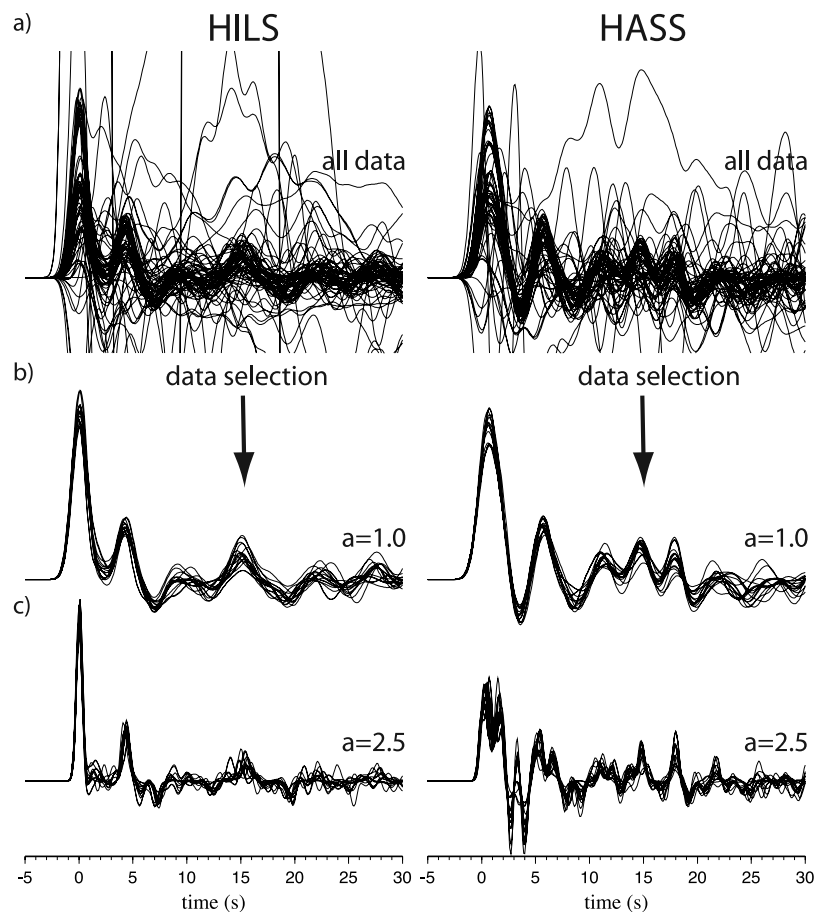


**Figure 3.** Two examples of receiver function estimates for the data from HILS and HASS. (a) Receiver functions from data corresponding to all events highlighted in Figure 2b (the northeastern back azimuths) for stations (left) HILS and (right) HASS. (b) Selected receiver functions after elimination of outliers and noisy records for the low-pass Gaussian filter width parameter  $a = 1.0$ . (c) Same as Figure 3b but for the low-pass Gaussian filter width parameter  $a = 2.5$ .

elimination of outliers and noisy records, we selected a final set of receiver functions for the low-pass Gaussian filter width parameter  $a = 1.0$  (Figure 3b) and  $a = 2.5$  (Figure 3c), which in time domain correspond to the width of the Gaussian pulse of about 1.67 and 2.64 s, respectively. We then stack the individual RFs to represent a mean receiver function for a given station. In Figure 3, we illustrate a difference in waveforms between HILS (Arabian Shield station) and HASS (Arabian Platform station). These differences become clear when higher frequencies are considered. For example, at HASS we observe a secondary arrival directly after the P wave, which is associated with a thick sedimentary layer. Even though HASS receiver functions are more complicated than other receiver functions due to the presence of sediments, we demonstrate in Figure 3c that our data quality and quantity is high enough that it is possible to extract a very coherent signal even at frequencies slightly above 1 Hz. This will be an important characteristic of our receiver function data, which will enable us to retrieve crustal models with high resolution and confidence.

## 2.2. Surface Wave Group Velocity Data

[15] We will combine the RFs with the fundamental mode surface wave group velocity tomography. The surface wave

tomography model was constructed from dispersion measurements from thousands of surface wave paths [Pasyanos *et al.*, 2001; Pasyanos, 2005]. Figures 4a and 4b illustrate the ray path coverage for 30 s Rayleigh and Love waves around the Middle East. Although seismicity in the region (indicated by the yellow circles) is confined mostly to the Zagros Mountains, Red Sea, Gulf of Aden, and Gulf of Aden, the events are well distributed around the Arabian Peninsula. Combined with the excellent station coverage (indicated by the red triangles), the path coverage (blue lines) is very dense, particularly for the Rayleigh waves.

[16] Figures 4c and 4d show maps of group velocities of Rayleigh and Love waves at 30 s. At this period, the Rayleigh waves are primarily sensitive to structure between 10 and 50 km depth, while the Love waves are sensitive to structure shallower than 30 km. Both maps clearly show fast group velocities beneath the thin crust of the Red Sea, Gulf of Aden, and Arabian Sea. Both maps also find slow group velocities beneath regions of thick crust and thick sediments. Because the Rayleigh waves are sensitive to deeper structure, thick crust (in the Zagros Mountains, for example) is emphasized in the first, while sedimentary basins (i.e., Eastern Mediterranean, Persian/Arabian Gulf, Mesopotamian Foredeep, Gulf of Oman) are emphasized in the

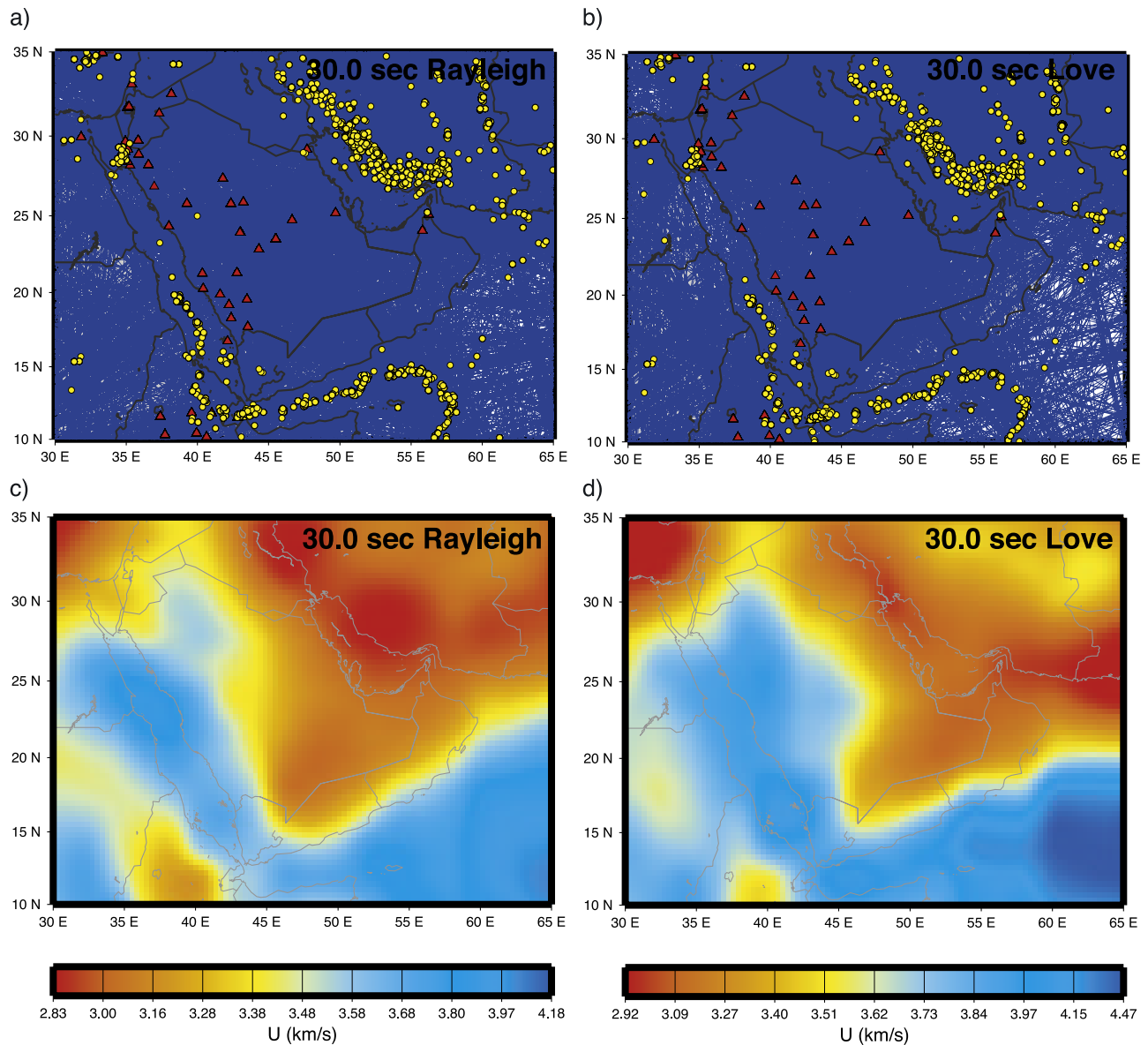


**Figure 4.** Map of 30-s surface wave group velocities. (a) Ray path coverage map of Rayleigh waves. (b) Ray path coverage map of Love waves. The triangles and circles denote the stations and earthquakes, respectively. (c) Rayleigh wave group velocities (in km/s) derived from tomographic inversion. (d) Love wave group velocities (in km/s) derived from tomographic inversion.

second. The boundary between fast and slow Love wave velocities in the Arabian Peninsula coincides very well with sedimentary thickness contours of the region. Because of the excellent coverage of the region, we can achieve spatial resolution that approaches  $1^\circ$ , at least for the shorter-wavelength surface waves. Uncertainties for the surface wave tomography are calculated using a bootstrapping approach [Pasyanos and Walter, 2002]. In general, the uncertainties of Rayleigh waves are smaller than those of Love waves, and the uncertainties of intermediate periods (20–60 s) are smaller than those of the shortest and longest periods. For example, for the 30 s Rayleigh waves the uncertainties are fairly small everywhere. The 30 s Love waves have small uncertainties everywhere on the Arabian Peninsula, but fall off (somewhat expectantly) in the Arabian Sea. The uncertainties of the 60 s Rayleigh waves are

higher than for 30 s Rayleigh, but still quite good (i.e., generally, uncertainties are smaller than 0.10 km/s). Similarly, the 60 s Love waves have higher uncertainties than 30 s Love, but (like the 60 s Rayleigh waves) still relatively small on the peninsula. We conclude that the uncertainties are fairly small because of the excellent ray path coverage in the region.

### 3. A Multistep Approach for Modeling Surface Wave Dispersion and Receiver Functions

[17] In order to solve jointly the surface wave dispersion and receiver function inverse problem for velocity structure, we employed a combination of a grid search and a standard iterative inversion technique including forward modeling (hereafter called MSA4 method, after multistep approach

that consists of four steps). The idea underlying MSA4 is to keep progressing gradually from the top to the bottom, solving for Earth's structure beneath a given station. Ideally, we seek for the simplest model that is able to fit the data. We invert for crustal structure first. The resulting models fit receiver functions and only short periods of surface wave group velocity dispersion curves. Because of the fact that receiver functions and short-period dispersion values are only weakly sensitive to upper mantle structure (assuming that there are no sharp discontinuities and that receiver functions are 30 s long), it is possible to perturb only the deeper part of the model (velocities and thicknesses of deeper layers) without degrading a fit for the receiver functions and dispersion at short periods from previous steps. Thus we solve for the crustal and upper mantle structure (to the depths of about 150 km), including crustal thickness, the extent and strength of lithospheric lid, the presence of low-velocity zones, and transverse isotropy, without the need to use strong geological and geophysical a priori constraints. A flowchart describing MSA4 method is presented in Figure 5.

### 3.1. Step 1: Joint Grid Search Inversion for the First Approximation of Crustal Structure

[18] In general, grid searches sample the parameter space bounded by the lower and upper limits looping over discrete values for each free parameter, and the fit statistics are evaluated at each grid point. On the one hand, an obvious advantage of a grid search method over other inversion techniques is that it provides goodness-of-fit statistics for an entire parameter space, within the limitations of its discrete nature. This is advantageous in situations where even an approximate structure under a station is not known a priori, for instance if one tries to invert for crustal structure based on observed receiver functions, while at the same time other geophysical and geological constraints on the crust do not exist. On the other hand, a serious disadvantage of grid search methods is in the fact that they are computationally intensive, especially in the framework of jointly inverting several independent data sets. Another disadvantage is that the structure of the parameter space might be finer than the selected grid spacing. Thus some assumptions are required in order to simplify the problem.

[19] We experimented with various  $V_p/V_s$  ratios in our modeling, from individual station to station, but we obtained good results with Poisson's ratio equal to 0.25 ( $V_p/V_s = 1.73$ ). The assumption that Poisson's ratio for sediments is equal 0.25 is arguable, but we tested the uncertainty in our final models for smaller values of Poisson's ratios and could not distinguish between which model is significantly better, based on the uncertainty in our measurements. Thicker sediments, say, 8 to 10 km, would have much more important effect. Thus, at the most basic level, we simplify a grid search, reducing the inverse problem to three layers in the crust and an additional layer below the crust extending down to 80 km depth, assuming Poisson's ratio  $\sigma = 0.25$  and the Birch's law for density [Birch, 1961]. The number of free parameters consequently reduces to  $2n + 1 = 7$ , where  $n$  is the number of layers (2 signifies shear wave velocity and thickness of each layer and 1 comes from shear wave velocity of the layer below the crust). We imposed minimal a priori constraints on the

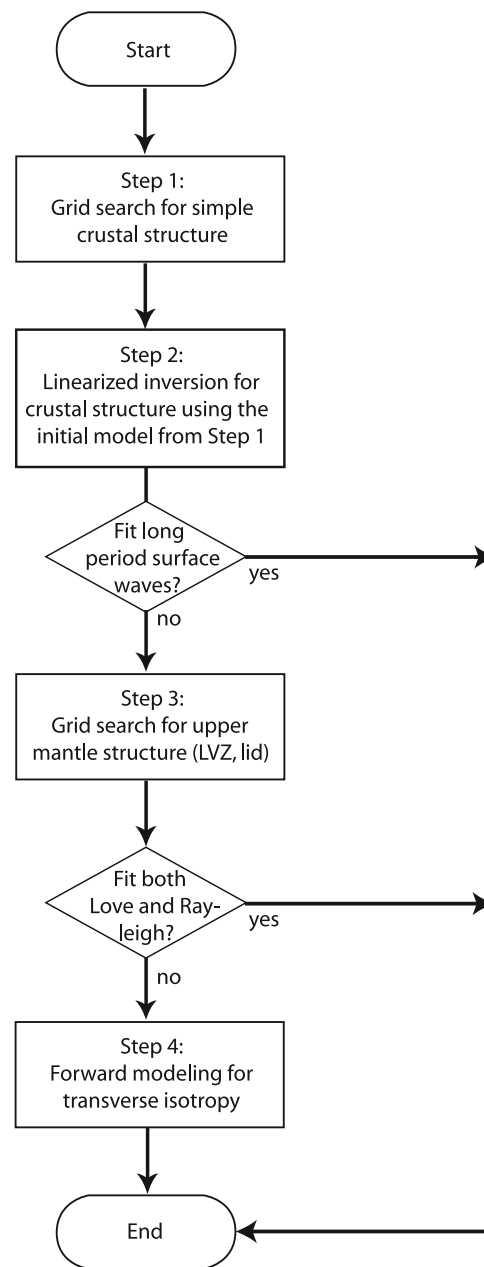


**Figure 5.** A flowchart demonstrating the four steps of the MSA4 method.

crustal thickness, with relatively coarse grid spacing (grid points at every 2 km for surface layer thickness, every 3 km for other layers, and 0.3 km/s for shear wave velocity). Given the number of possible models the computation of synthetics for receiver functions and surface wave dispersion curves is still too large to do for each station on a Sun/Unix work station. However, we solved this problem by computing and storing a database of synthetic receiver functions and synthetic dispersion curves from a number of models according to "3 crustal layers + 1 mantle layer" scheme. This is done for receiver functions with Gaussian filter width parameter  $a = 1.0$  and duration of 30 s, for a range of ray parameters and for both Love and Rayleigh group velocity dispersion synthetics. We used a reflectivity

**Table 1.** Parameters That Characterize Each Layer in the Initial Grid Search Inversion Scheme (Step 1)<sup>a</sup>

Layer	Thickness	V <sub>s</sub> Velocity, km/s	Δh, km	Δv, km/s
1	h <sub>1</sub> = 0 to 12 km	V <sub>1</sub> = 2.7–4.2	2	0.3
2	h <sub>2</sub> = 3 to H <sub>MOHO</sub> – (h <sub>1</sub> + h <sub>3</sub> )	V <sub>2</sub> = 3.0–4.5	3	0.3
3	h <sub>3</sub> = 3 to H <sub>MOHO</sub> – (h <sub>1</sub> + h <sub>2</sub> )	V <sub>3</sub> = 3.3–4.8	3	0.3
4	h <sub>4</sub> = 80 – H <sub>MOHO</sub>	V <sub>4</sub> = 4.3–4.7	–	0.2

<sup>a</sup>Thickness and shear wave velocity of each layer can vary with a step specified in Δh and Δv columns, respectively.

synthetic seismogram algorithm by G. Randall, based on the method developed by Kennett [1983] and a time domain deconvolution to produce synthetic receiver functions in the same manner as it was done for the seismograms. For surface wave group velocity dispersion, we used algorithm DISPER80 developed by Saito [1988]. The medium below 80 km depth, which was a half-space in the creation of receiver functions synthetics, here is replaced by a series of layers with PREM thicknesses and velocities [Dziewonski and Anderson, 1981].

[20] The ranges of the grid search for each layer are given in Table 1. For a given ray parameter and our grid search specification, the number of synthetic receiver functions and corresponding dispersion curves is slightly over 198,000. It took more than 2 days of CPU time to compute the database of synthetic receiver functions for a single value of the ray parameter, and about 8 hours to populate corresponding database of synthetic dispersion curves (which has no dependence on ray parameter) on the work station “Sun Blade 2000.” It is possible by investing some additional CPU time, to extend the existing database by more closely spaced grid point synthetics.

[21] With the current grid spacing (specified in Table 1), it takes about 1.5 hour to run a grid search algorithm on Sun Blade 2000 by calculating statistics for each model. Root-mean-square (RMS) and variance reduction (VR) for each model are calculated as a measure of misfit according to the following expressions:

$$\text{RMS} = \sqrt{\frac{\sum_{i=1}^N w_i (\text{obs}_i - \text{theor}_i)^2}{N}}$$

$$\text{VR} = \left\{ 1 - \sqrt{\frac{\sum_i (\text{obs}_i - \text{theor}_i)^2}{\sum_i \text{obs}_i^2}} \right\} 100\%$$

[22]  $N$  is the number of selected periods for Love or Rayleigh wave dispersion at a given station. Typically, we consider 11 discrete periods spanning from 20 to 70 s for Love waves, and 20 discrete periods spanning from 7 to 100 s for Rayleigh waves, but  $N$  is smaller for stations MEZE and HITJC due to the fact that we do not have as reliable dispersion measurements at the shortest periods. The obs and theor are the observed and theoretically predicted points, respectively, for the both receiver functions and surface wave dispersion.  $w$  is defined as  $1/e$  (where  $e$  is the error of each point in surface wave dispersion measurements) and is a relative weight of each velocity measurement

in the dispersion. If there is a large misfit at only one single period of the group velocity dispersion, we infer from the above formula for RMS that this will significantly penalize the result. However, the above formula for VR secures that the result will not be significantly penalized if there is a large misfit at one point. Therefore VR is more appropriate measure of misfit than RMS for continuous waveforms (receiver functions) with much larger number of points than in discrete dispersion measurements, where it is important to fit the general character of the waveform. RMS and VR expressions are both used as criteria for selection and plotting small arbitrary percentages of the best models. When only one data set (receiver function or Love or Rayleigh wave dispersion) is considered, it is straightforward to select a desired percentage of the best models. When all the three data sets are combined, we must trade off the fit to each individual data type in order to find a range of appropriate models. Therefore the percentage of the best models that fit one data set is gradually increased until common models are found that simultaneously fit all data sets. In practice, this means that we sacrifice the quality of the fit to one single data set for a reasonable fit of all data sets. The importance of fits of each data set is achieved by adjusting different percentages of the best models. For example, if a good fit to the receiver function data is desired, the percentage of the best models fitting receiver functions is set to be small (e.g., 1%), while the percentage of the best fitting models for surface waves is gradually increased (e.g., up to 50%) until a desired number of common models are found to fit all data sets.

[23] The resulting models consisting of three-layer crust and a half-space are often too simplistic. We note, however, that some excellent matches to the data were found, particularly in cases when only receiver function or only surface wave data (either Love or Rayleigh wave dispersion) are considered. This is illustrated in Figures 6 and 7 for stations HILS (Figures 6a and 7a), AFFS (Figure 6b), and HASS (Figure 7b). Initial grid searches for receiver functions are done using  $a = 1.0$  because the goal is to find a good starting model. The observed receiver functions (Figure 6) are fit well for HILS with three-layer model of the crust, with some larger uncertainty in top 15 km in the best models, but resolving the Moho depth. The crustal structure is somewhat more uncertain for AFFS, although the fits to the waveforms that are achieved with three-layer model are good and Moho depth seems to be well resolved with uncertainty of several kilometers. Surface wave dispersion curves (Figure 7) are fit well for station HILS, but resulting best models are more variable than for the receiver function fits. This confirms a well-known property of surface waves being more sensitive to the absolute velocity structure, but without constraints on the depths of discontinuities. For station HASS, an additional complexity stems from the fact that the best models fail to fit the dispersion at long periods due to the overly simplistic half-space mantle (55–70 s for Love and 60–100 s for Rayleigh waves). In general, fitting the group velocities is challenged by the fact that the group velocity curves are scattered, particularly for longer periods.

[24] When all the three data sets are combined, it becomes clear that much finer details in structure below a given station are required in order to fit these data sets simultaneously with reduced variance. Examples of best fits for

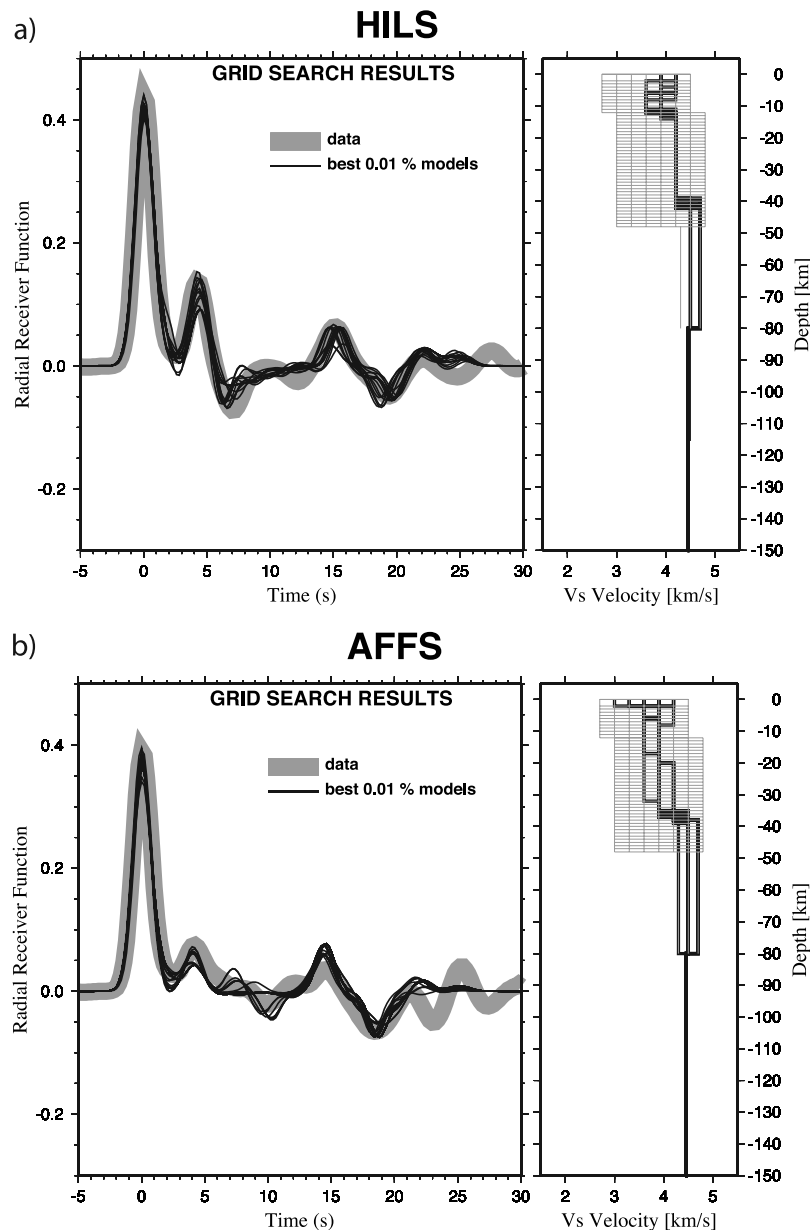


**Figure 6.** Grid search results for lithospheric structure after modeling the observed receiver functions for a low-pass Gaussian filter width parameter  $a = 1.0$  for (a) HILS and (b) AFFS, two stations located in the Arabian Shield. Thick gray line is a stacked and averaged observed receiver function and thin black lines are (left) modeled receiver functions and (right) corresponding shear wave velocity profiles for the best 0.01% models obtained in the grid search. The range of grid search is shown on the right by thin gray lines.

stations: HILS (Figure 8a), AFFS (Figure 8b), and KBRS (Figure 8c) are given. Here we show best fit models for receiver function and surface wave joint grid search inversion. For station HILS, grid search returns relatively good fits even if all three data sets are inverted for simultaneously. This fit can be further improved by increasing the number of free parameters; however, the data suggest that the lithospheric structure under this station is simple and the data can be explained with a small number of parameters. However, for the other two stations shown, a satisfactory joint fit of receiver functions and surface wave dispersion is not possible. At station AFFS this manifests in overestimated velocities in the dispersion curve at long periods. At

station KBRS the misfit is even more drastic, with the velocities at all periods of Love wave dispersion being largely underestimated. This is a challenge that requires extending the simple grid search with several additional steps, which will be described below.

[25] At this stage in MSA4, we have an adequate starting model for further improvement. In particular, for receiver functions, we focus on matching the amplitudes and character of the first (direct P) and the second peak (Ps), as well as the later cycle (PpPms and PpSms + PsPms) mostly sensitive to the velocity contrast at Moho. In cases where we were not able to fit all three data sets simultaneously, we select models that fit receiver functions and Rayleigh wave group velocity

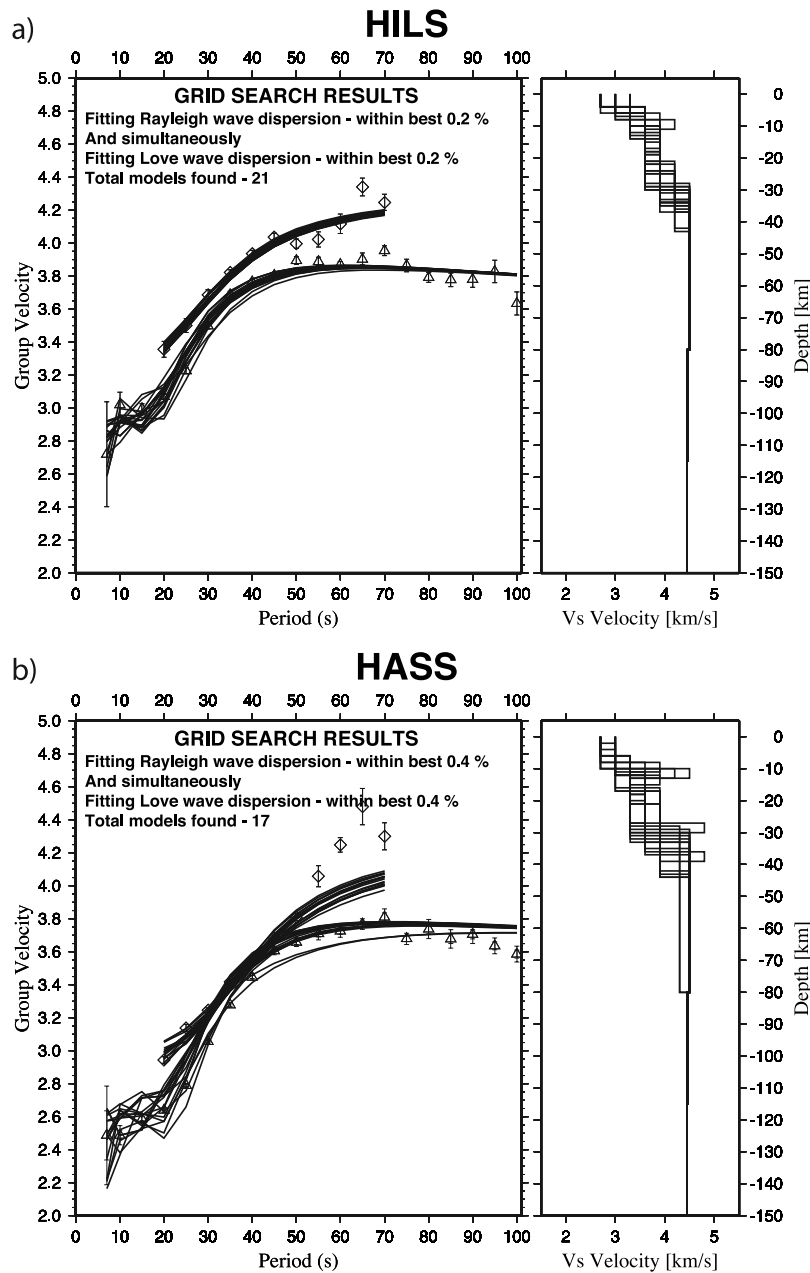


**Figure 7.** Grid search inversion results for lithospheric structure after modeling the observed Rayleigh wave (triangles) and Love wave (diamonds) group velocity dispersion at HILS and ADFS, the two stations also shown in Figure 6. Black lines are (left) modeled dispersion curves and (right) corresponding shear wave velocity profiles for the best 0.2% (for HILS) and 0.4% (for ADFS) models obtained in the inversion. The  $\pm 1$  standard deviation bars are shown on SWGV data.

dispersion since both are sensitive to vertically polarized S waves. The selection of Rayleigh over Love wave group velocity dispersion at this point is justified because the measurement errors at short periods are smaller for Rayleigh than Love wave group velocities, and we preserve data points at 7, 10 and 15 s only for Rayleigh waves.

### 3.2. Step 2: Linearized Iterative Joint Inversion for Crustal Structure

[26] Step 2 involves using a satisfactory model from step 1 as a starting model for an iterative joint inversion method [Julià *et al.*, 2000] that converges quickly toward a result.

By deriving a starting model (through a grid search) and by providing it as an input for standard linearized inversion technique, we avoid a problem of being biased toward an unrealistic starting model, possibly shifting final velocities toward a wrong direction and not obtaining the best variance reductions. The method by Julià *et al.* [2000] is based upon an iterative damped least squares scheme. It allows, by using a priori damping and influence parameters, an elegant control of smoothness and manipulation of relative weights given to independent data sets (for details, see Julià *et al.* [2000]). By increasing the model parameters (and thus sacrificing the simplicity of initial structural

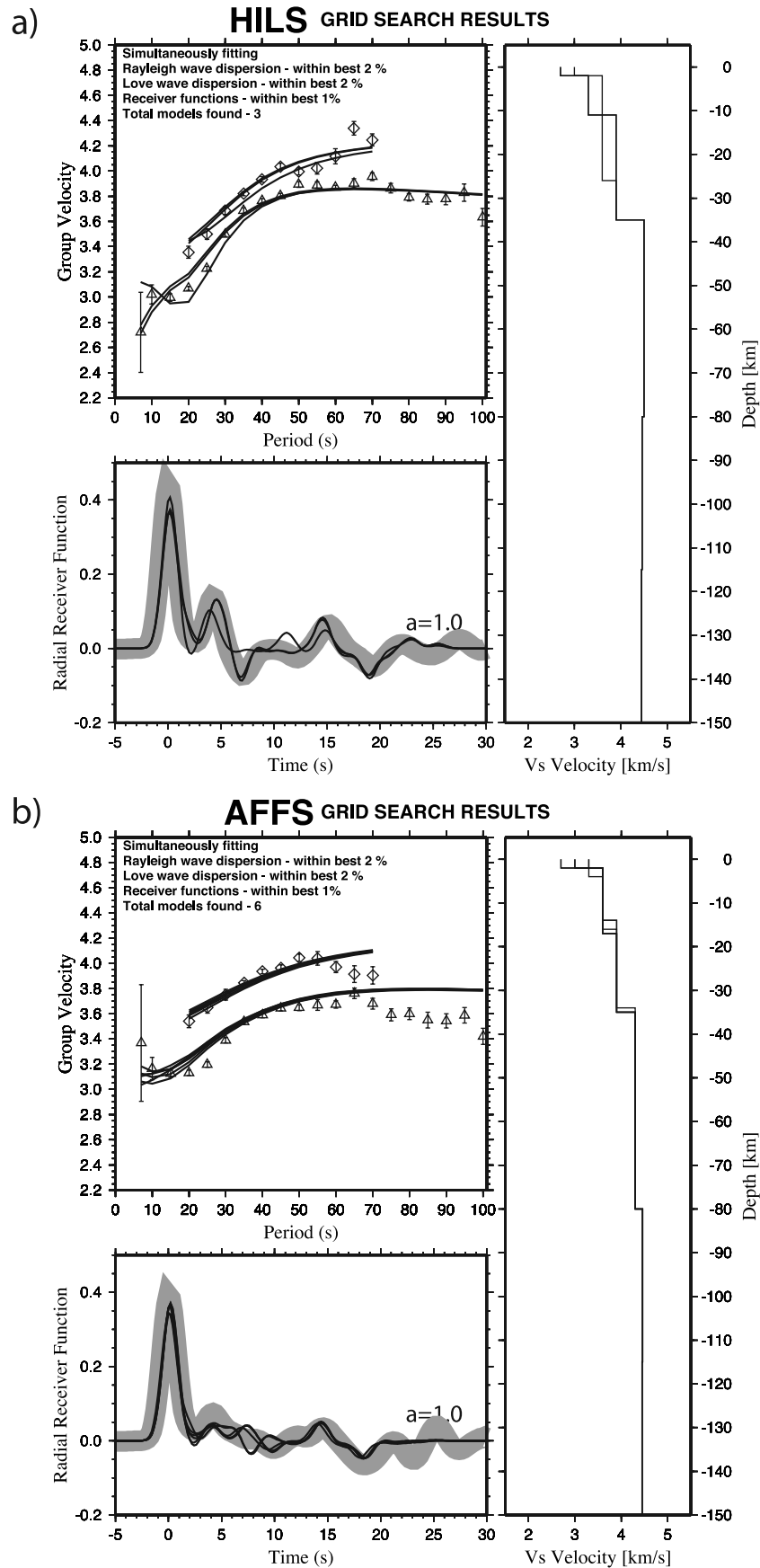


Figure 8

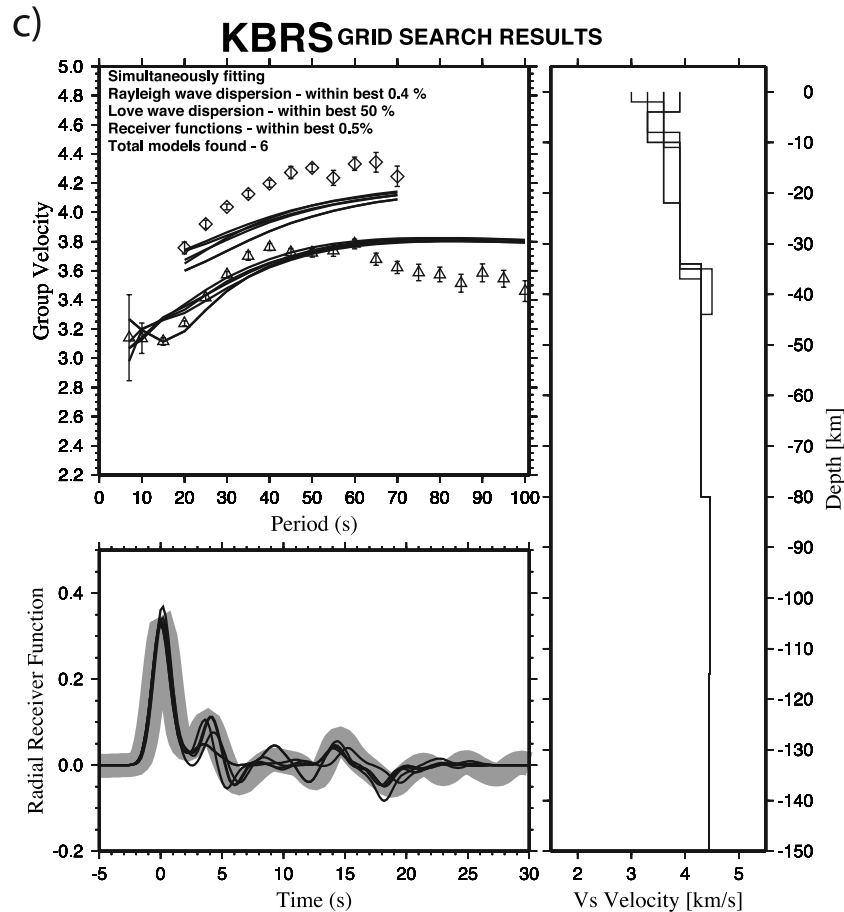


Figure 8. (continued)

models), we used this method to further improve the receiver function, as well as the dispersion fit at short periods. In this step, we invert receiver function data for both  $a = 1.0$  and  $2.5$ .

[27] An example of a fit at short periods after the iterative inversion runs is shown in Figure 9. The fit for station AFFS shown in Figure 9a is quite good for the receiver functions and the dispersion at short periods only ( $T < 70$  s). In order to model the complexity of surface wave dispersion curves at short periods, we had to introduce more layers in the model, to represent a gradient in the sediments as well as a gradational Moho. *Julià et al.* [2000] presented a similar fit for station AFIF of the PASSCAL deployment; however, their fits were achieved using only periods of up to 60 s.

[28] The fit for station KBRS is shown in Figure 9b. When attempting to jointly fit receiver functions and surface wave dispersion curves for both Love and Rayleigh waves, the method was unstable even when more weight was given to fitting surface wave dispersion and when the smoothness

parameter was constrained to be very small (higher contrasts in velocities were allowed). One such fit is represented in Figure 9b by dashed lines. While fitting the receiver functions well, the model is clearly unable to fit jointly Love and Rayleigh group velocity dispersion. Therefore we constrain the joint inversion to fit only Rayleigh wave dispersion and the receiver functions, which is shown by thick black line in Figure 9b.

[29] Very frequently, particularly for the stations located in the Arabian Shield, the observed surface wave group velocities are systematically lower than predicted ones at intermediate and long periods of the surface wave group velocity dispersion (i.e.,  $T > 60$  s). We found it very challenging in practice to fit surface wave dispersion at long periods, without introducing features like a lithospheric lid and a low-velocity zone under the lid. We also found it impossible to produce synthetics that would fit simultaneously Love and Rayleigh wave group velocity dispersion, and at the same time not degrade a fit to the receiver

**Figure 8.** Results of grid search inversion (step 1) for lithospheric structure after jointly fitting the observed Rayleigh wave (triangles) and Love wave (diamonds) group velocity dispersion and the observed receiver functions (thick gray lines). Results are shown for (a) HILS (b) AFFS, the same two stations featured in Figures 6 and 7, (c) KBRD, an additional station located in the Arabian Shield. Black lines are (left) modeled dispersion curves and receiver functions and (right) corresponding shear wave velocity profiles for the best models (percentage varies from station to station) fitting simultaneously Love and Rayleigh wave dispersion and receiver functions. Note that fits are not very accurate owing to a simple crustal structure used in modeling.

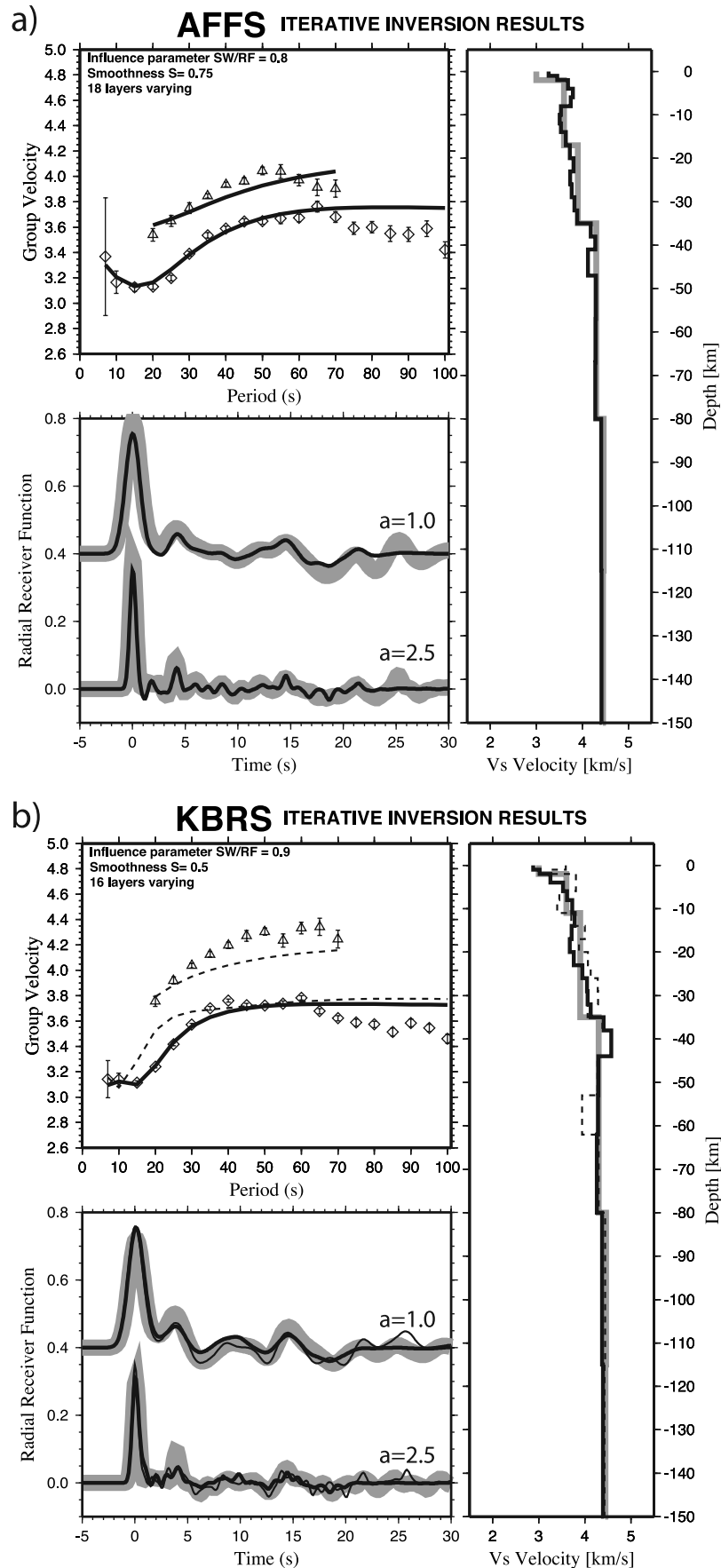


Figure 9

functions. Therefore it is necessary to carry out an additional grid search for mantle velocities with a goal of obtaining fits at the long-period part of the observed dispersion curves.

### 3.3. Step 3: Additional Grid Search for Long-Period Dispersion Fit

[30] With a well-constrained crustal velocity structure from the previous steps, the trade-off between crustal and mantle structure is reduced. In the third step, we introduce new free parameters such as the depth, vertical extent and velocity gradient between the lithospheric lid and the asthenospheric low-velocity zone (LVZ). We choose a trapezoidal shape of velocity as a function of depth to describe a possible LVZ, with linear gradient between the maximum and minimum velocity, in order to avoid introducing new conversions or reverberations in the RFs. Since these new parameters are not entirely independent, and we assume that the shear velocity profile in the LVZ looks like a trapezoidal function (first decreasing, constant, and increasing with depth), the final number of free parameters in this stage of the problem can be reduced to 4: (1) shear wave velocity below the Moho; (2) the depth at which the LVZ starts (which defines the thickness of the lithospheric lid); (3) the minimum shear wave velocity in the LVZ; and (4) the vertical extent of the LVZ. The grid search thus consists of comparing about five thousand synthetics with the observed data and calculating statistics, which took about 15 min CPU time on Sun Blade 2000 station. Figure 10 shows the best models for the stations AFFS and KBRS, shown also in the previous steps.

[31] This step results in models that fit the dispersion of Rayleigh waves at longer periods, and only slightly degrade the shorter-period dispersion curve and receiver function fits (compare Figures 10 and 9). At station AFFS, the overall fit now looks much better than that presented in the step 2, mainly stemming from improvement of fit for the dispersion at periods longer than 70 s for Rayleigh waves. In this case, no prominent lithospheric lid nor the LVZ was found in the best fitting models for AFFS; however, the velocity throughout the upper 100 km of the mantle remain slow (4.2–4.3 km/s), suggesting that the upper mantle is anomalously hot.

[32] The fits for long-period Rayleigh wave group velocity dispersion dramatically improve for station KBRS, too. This results from a uniform velocity lithospheric lid and pronounced LVZ, which starts at depths about 70 km and extends to depths about 150 km. However, it becomes evident here that anomalously low Love wave group velocity values require additional adjustments in velocity struc-

ture, which has not been addressed in the receiver functions studies for this area.

### 3.4. Step 4: Forward Modeling: Fine Tuning of Velocity Structure, First-Order Modeling of Transverse Isotropy in the Upper Mantle and Final Models

[33] In the fourth and final step, we perform a forward modeling of velocity and anisotropy structure in the upper mantle. Our goal is to further improve fits to the surface wave dispersion while simultaneously preserving the fits to the receiver functions achieved in the previous steps of our approach. Through the first three steps, we tried to fit our data by structure in the crust and the upper mantle. However, it is not until this step in our procedure, that both Love and Rayleigh wave group velocity discrepancy could be explained significantly better, allowing for the existence of polarization anisotropy in the upper mantle and possibly even in the lower crust. Polarization anisotropy is the simplest parameterization that jointly satisfies Love and Rayleigh wave group velocity discrepancy and this has been long known [e.g., *Anderson, 1961; Dziewonski and Anderson, 1981*]. Polarization anisotropy has been used for mapping regional variations in transverse isotropy [e.g., *Gaherty and Jordan, 1995; Gaherty, 2004*]. A form of polarization anisotropy, shear wave splitting was also used to study anisotropy in the crust and mantle [e.g., *Silver and Chan, 1988*]. For a more detailed review of mantle anisotropy, see, for instance, *Silver [1996]*. In our forward modeling, we are not able to resolve well the fine details of radial dependence of amplitudes of anisotropy; however, we can resolve quite well its sign (positive for  $v_{SH} > v_{SV}$  and negative for  $v_{SH} < v_{SV}$ ) and its radial extent. Therefore the radial profiles of transverse isotropy (with gradual increase, flat value and decrease) are somewhat arbitrary. Sensitivity kernels of surface waves are quite complex and we limit our modeling efforts only to introducing simple anisotropy function of depth. We used forward modeling to obtain our final models for 10 stations in the Arabian Peninsula and present these in the next section.

### 3.5. Lateral Resolution of Surface Waves and Receiver Functions

[34] One concern is that the difference in resolution of RFs and SW data may produce artifacts during the joint inversion when small-scale variations in crustal structure observed with the RF data may be mapped into apparent small-scale variation of the mantle structure. Therefore we first compared the resolutions of Love and Rayleigh surface waves with lateral resolution of teleseismic receiver functions in the crust. The wavelengths of Love and Rayleigh

**Figure 9.** Iterative inversion results (step 2) for lithospheric structure after jointly fitting the observed Rayleigh wave (triangles) and Love wave (diamonds) group velocity dispersion and the observed receiver functions (thick gray lines) for low-pass Gaussian filter width parameters  $a = 1.0$  and  $a = 2.5$ . Results are shown for (a) AFFS and (b) KBRS, the same two stations featured in Figures 8b and 8c. Black lines are (left) modeled dispersion curves and receiver functions and (right) corresponding shear wave velocity profiles for the best models (percentage varies from station to station) fitting simultaneously Love and Rayleigh wave dispersion and receiver functions. For KBRS data, thin lines represent a simultaneous fit to all three observed data sets, as in Figure 9a, while thick line represents a simultaneous fit to only the observed receiver functions and Rayleigh wave group velocity dispersion. Compare this figure with Figures 8a and 8b to see the improvement of fits. Note that for AFFS and KBRS data, Rayleigh wave group velocity dispersion is not well fit at higher periods.

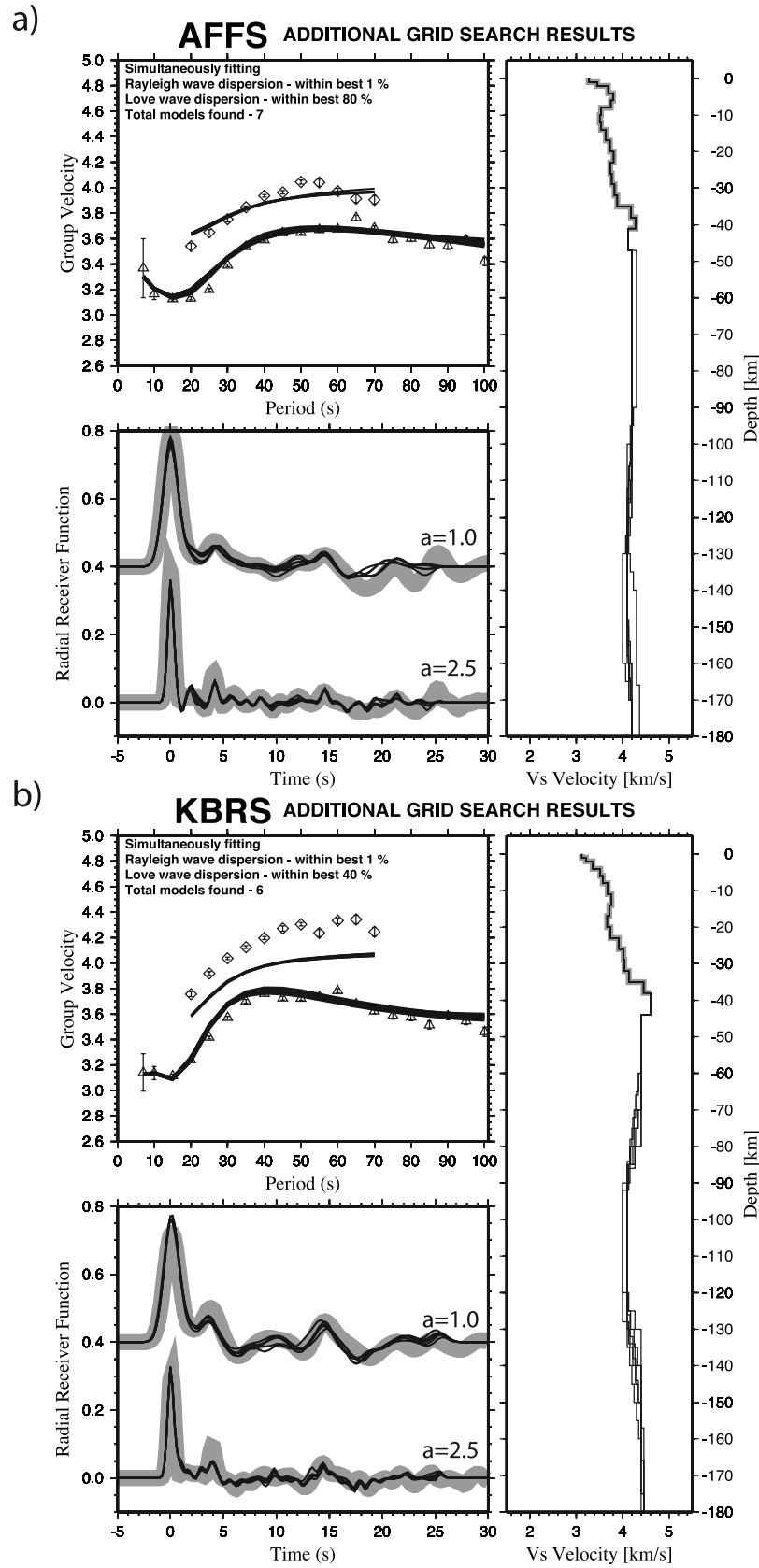


Figure 10

waves (periods multiplied with average group velocity) for the periods between 7 to 20 s range from 20 to 65 km and from 19 to 60 km for Love and Rayleigh waves, respectively. For the receiver functions, we can consider geometry of a multiple ray called PpPmp, as a useful bound on the lateral sampling of the structure. For the crustal thicknesses ranging between 30 and 45 km, we obtain values for the lateral resolution of the receiver functions between 24 and 36 km for the ray parameter 0.04 s/km and between 38 and 57 km for the ray parameter 0.06 km/s. Therefore the lateral resolution of surface waves and teleseismic receiver functions is very comparable in the crust. These data have complementary spatial resolution and can produce a model with well-constrained depths of boundaries and absolute velocity in the crust and upper lithospheric layers.

[35] The influence of the deep lithospheric layers can only be seen in our data through the variations in longer-period surface wave dispersion. However, since we first solved for the crust using two independent data sets, we can model variations in the long-period surface wave dispersion by perturbing velocities in the lower lithospheric layers, without the concern that there would be trade offs introduced from the upper lithospheric layers.

[36] Another concern is the resolution of the surface waves in the mantle, and whether the variations in mantle structure we might obtain between the stations located in the northern and southern part of the Red Sea are real. The distance between stations BLJS and NAMS from stations YNBS and KBRS (about 618 and 793 km for the shortest and longest distance, respectively) clearly exceeds that of the wavelength of Love and Rayleigh waves at long periods (for example, at 60 s, the wavelengths are about 242 and 225 km for Love and Rayleigh waves, respectively). Therefore the stations at the northern and the southern part of the Red Sea we use are separated enough for lateral heterogeneities in the mantle to impact long-period surface wave group velocities. In order to demonstrate this quantitatively, we performed a checkerboard test of the surface wave tomography at 30 and 60 s. The cells in the checkerboard tests for which we obtained a good resolution on the Arabian Peninsula were 4 degrees wide, therefore almost by a factor of two smaller than the shortest distance between the stations displaying differences in dispersion of surface waves. This shows that the sensitivity of the surface wave dispersion considered is greater than the station spacing, even for the 60-s periods.

#### 4. Results

[37] Figures 11a–11e illustrate the final fit to the data and our best proposed model for stations AFFS, ARSS, BLJS, HASS, HILS, HITJC, KBRS, MEZE, NAMS, and YNBS. Station AFFS (Figure 11a) is located in the eastern part of the Arabian Shield. As expected, we do not observe any

sediments. The upper crust is characterized with a small drop in shear wave velocities at about 8 km depth and gradual increase to about 3.9 km/s in the layer above Moho. The crustal thickness is about 35 km, with a fairly pronounced contrast characterizing Moho. *Al-Damegh et al.* [2005] and *Sandvol et al.* [1998b] estimated Moho depths at 32 and 39 km, respectively, from their receiver function studies. Although they interpret this discrepancy by the fact that the noise level of the recorded waveforms at that station changed, we think that surface waves add an important constraint in resolving the crustal structure and therefore we prefer depth of 35 km. From our best model, we conclude that the lithospheric lid is either absent or thin (20 km). More striking feature in our model is very low value of shear wave velocity in the mantle (4.1 km/s). A layer of transverse isotropy in the zone just below Moho slightly improves fits for Love wave dispersion at intermediate periods ( $T = 35\text{--}60$  s). We present a model in which a narrow zone of transverse isotropy extends to about 20 km below Moho ( $v_{SH} > v_{SV}$  about 6%) gradually ceasing with depth.

[38] Station ARSS (Figure 11b) is located about halfway between stations AFFS and HILS, situated slightly eastward but still in the Arabian shield. The RFs are similar to those observed at HILS, and SWGV dispersion curves look transitional between those observed at AFFS and HILS. Again, the upper crust is characterized by a strong transition in seismic velocity at 8 km depth and a slightly more varying lower crust than for AFFS. Our preferred model has a 40 km thick crust and a relatively pronounced Moho, with a thin lithospheric lid extending 10 km below Moho, even though it is difficult to resolve the mantle lid with such low velocities. In contrast to station AFFS, but consistent with station HILS, no transverse isotropy is needed to simultaneously explain Love and Rayleigh dispersion data. While a thin lithospheric lid is consistent with our preferred model for AFFS, the lack of transverse isotropy is comparable with HILS model. Another similar feature to AFFS is a broad zone of low shear wave velocity in the upper mantle (4.3 km/s) extending down to the bottom of our model. It appears that the lithospheric lid thickens significantly somewhere between ARSS and HILS and that the transverse isotropy seen at AFFS does not exist at ARSS.

[39] Station BLJS (Figure 11c) is located in the western part of the shield. Besides YNBS and NAMS, this is the closest station to the Red Sea that we analyzed. We found gradually increasing velocity in the upper crust, with maximum between 15 and 20 km, and decreasing slightly below these depths. This middle crust maximum is somewhat less pronounced than in the neighboring station NAMS because lower crust velocities for BLJS are higher; however, some resemblance in the final velocity profiles between the two stations exists. The Moho is estimated at 38 km depth, which is in excellent agreement with the study

**Figure 10.** Best fits to the observed Rayleigh wave (triangles) and Love wave (diamonds) group velocity dispersion and receiver functions (thick gray lines) after performing an additional grid search (step 3) for the lithospheric structure. In this step, we use the best crustal model from step 2 (thick gray line in velocity profiles), which we keep unchanged, and search over a parameter space consisting of additional four free parameters describing a low-velocity zone in the mantle. Compare this figure with Figure 9 to see the improvement of the fits at longer periods of dispersion. Note a poor fit of Love wave dispersion observed at KBRS systematically at all periods.

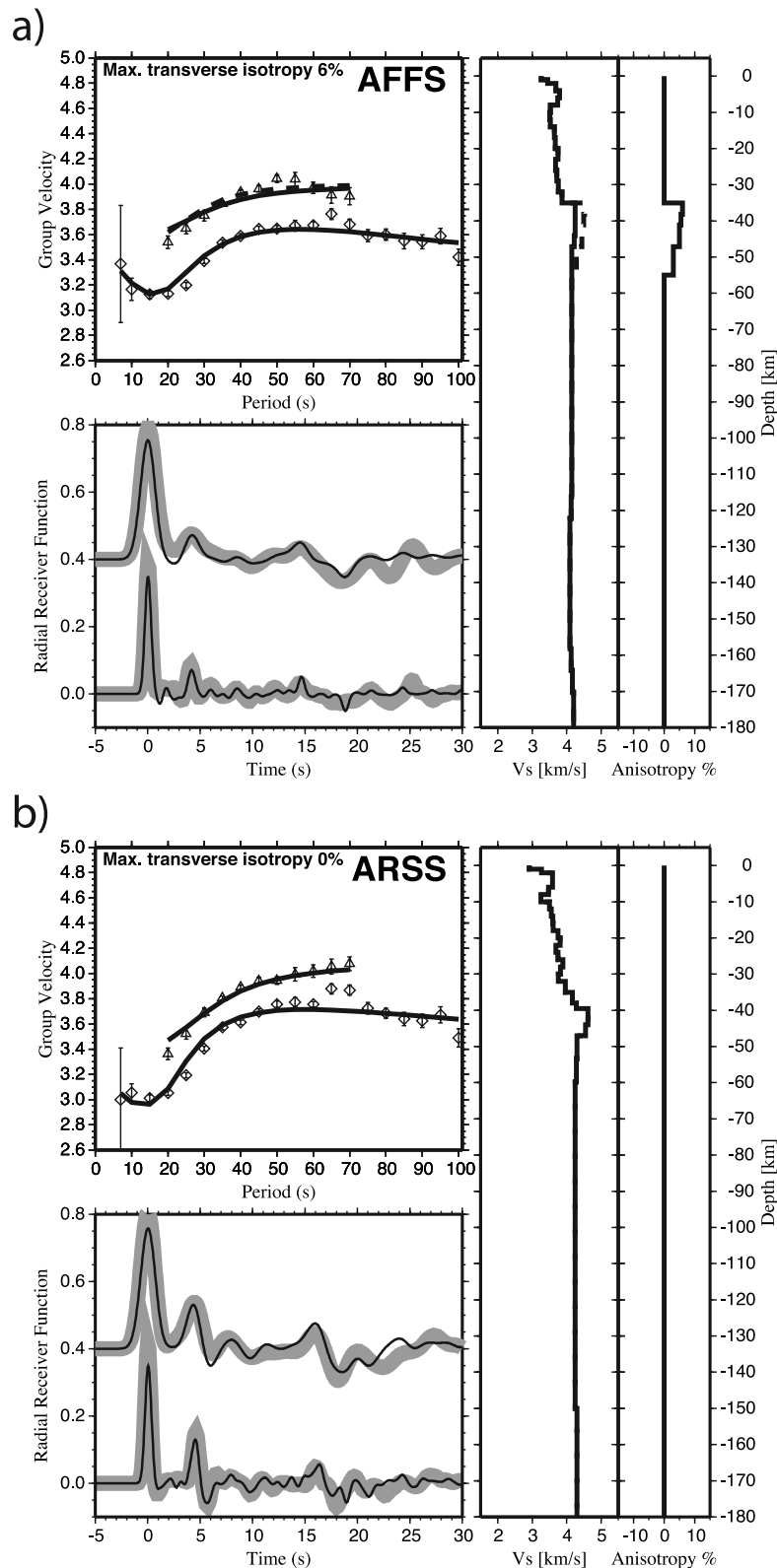


**Figure 11.** Results for lithospheric structure of the Arabian Peninsula at 10 stations after forward modeling for velocity and anisotropic structure (step 4), a final step of MSA4. The stations are presented in an alphabetical order. In addition to symbols described in previous figures, dashed line indicates the best fitting shear velocity model, as well as the best fitting Love wave group velocity dispersion when polarization anisotropy is included in modeling. Compare results for stations AFFS and KBRS with Figure 10 to see the improvement of the fits. Also compare with Figures 8a and 8b to see the improvement of the fits relative to an early stage of modeling.

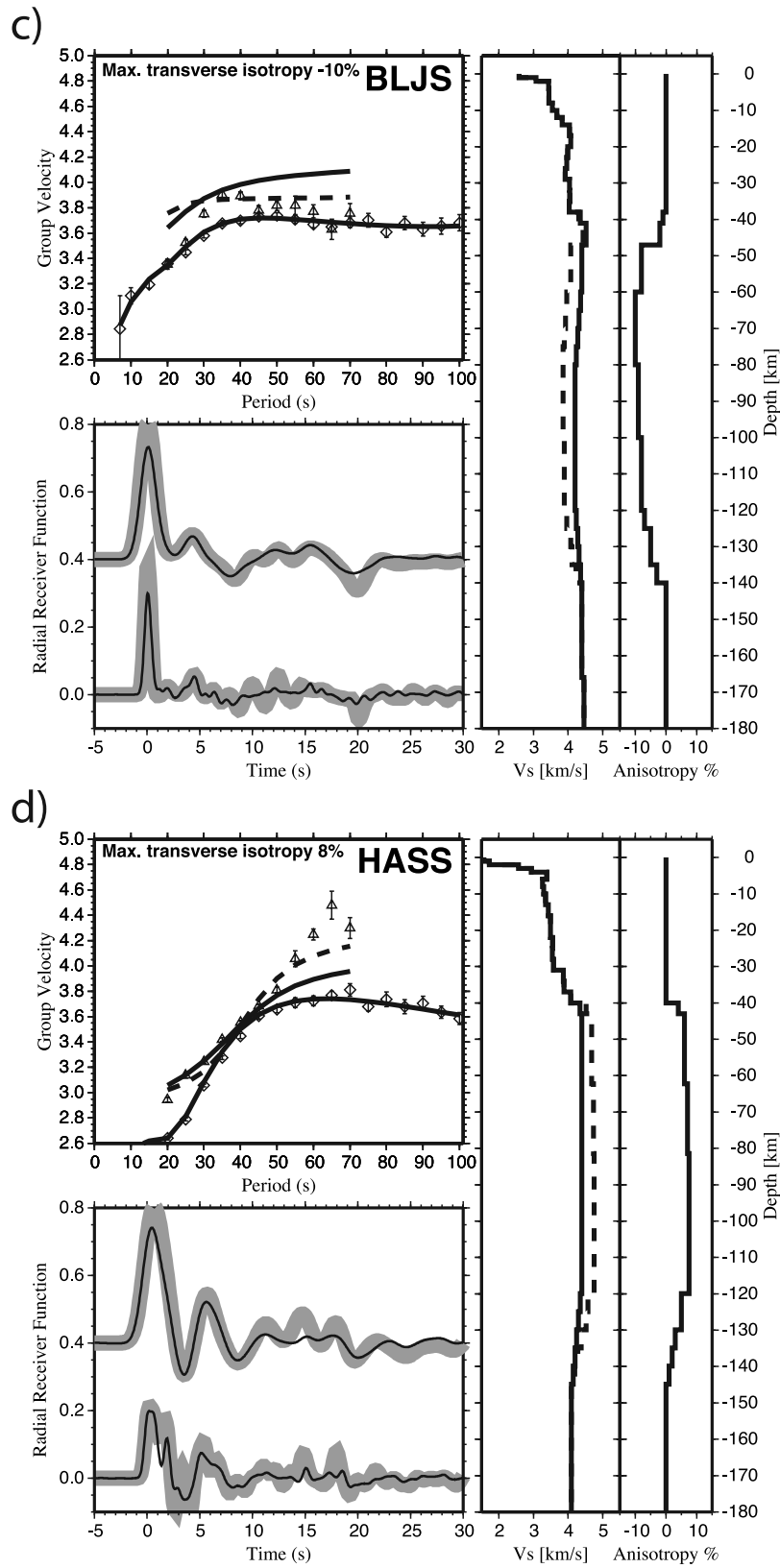


Figure 11. (continued)

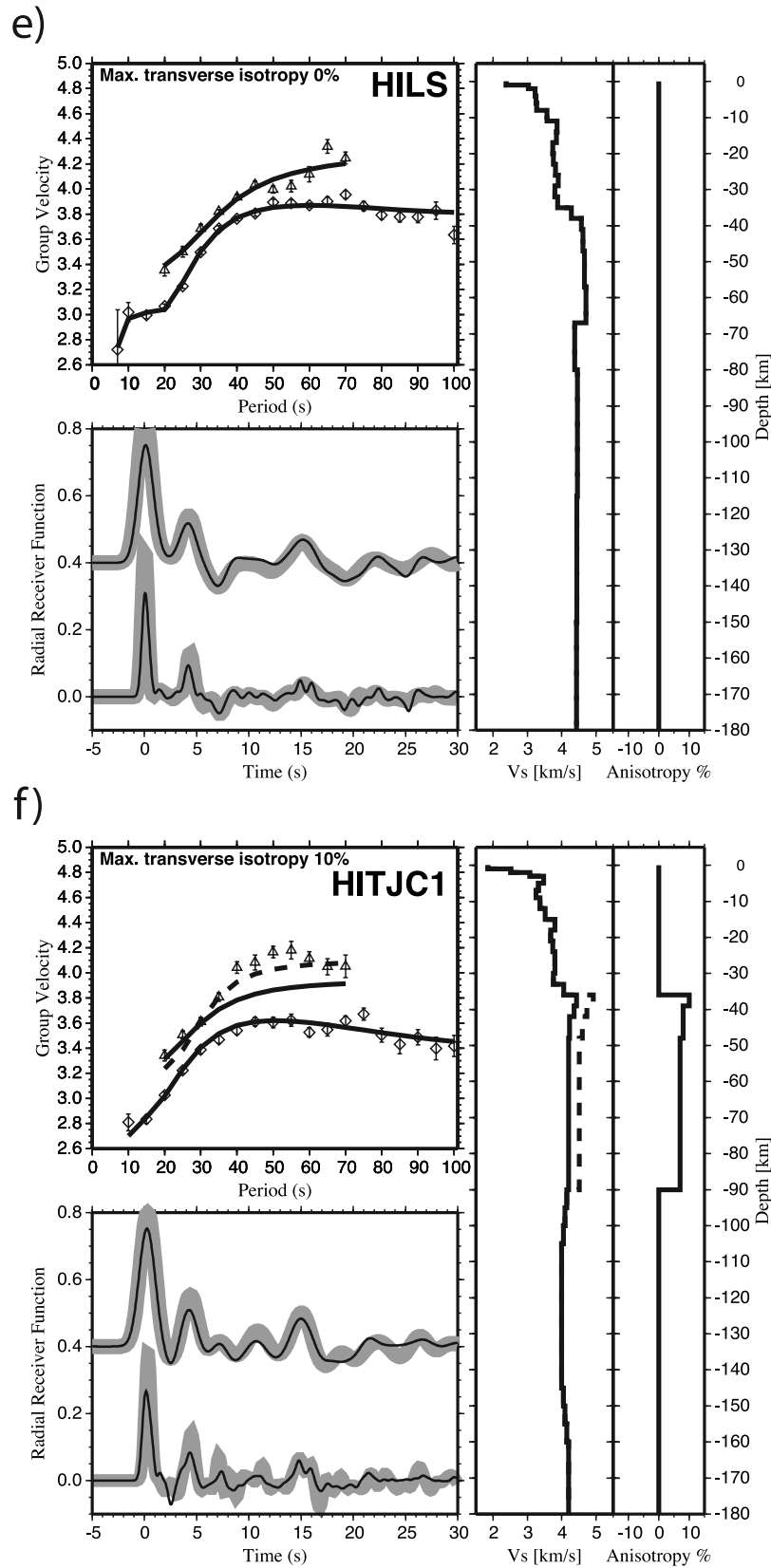


Figure 11. (continued)

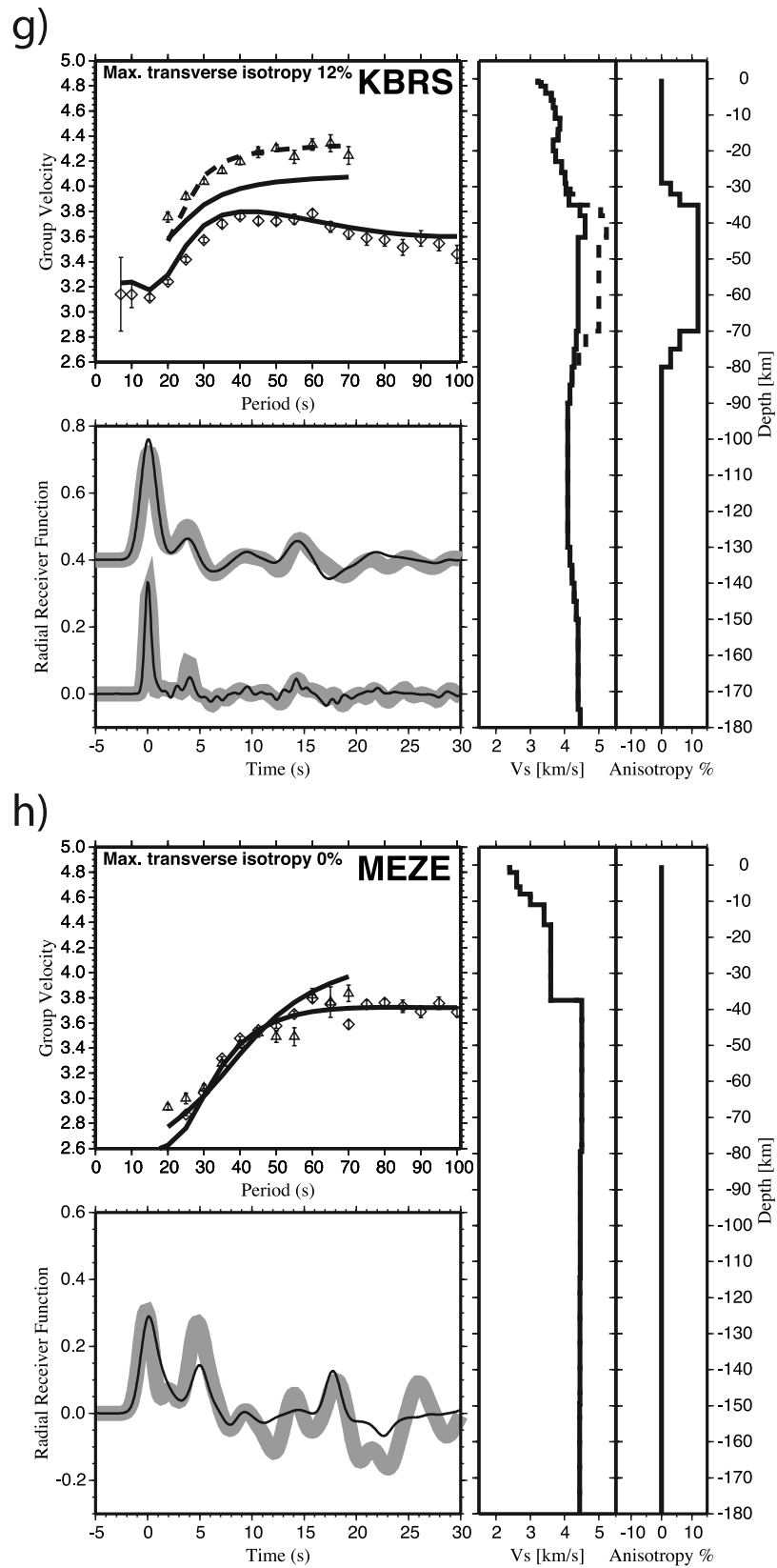


Figure 11. (continued)

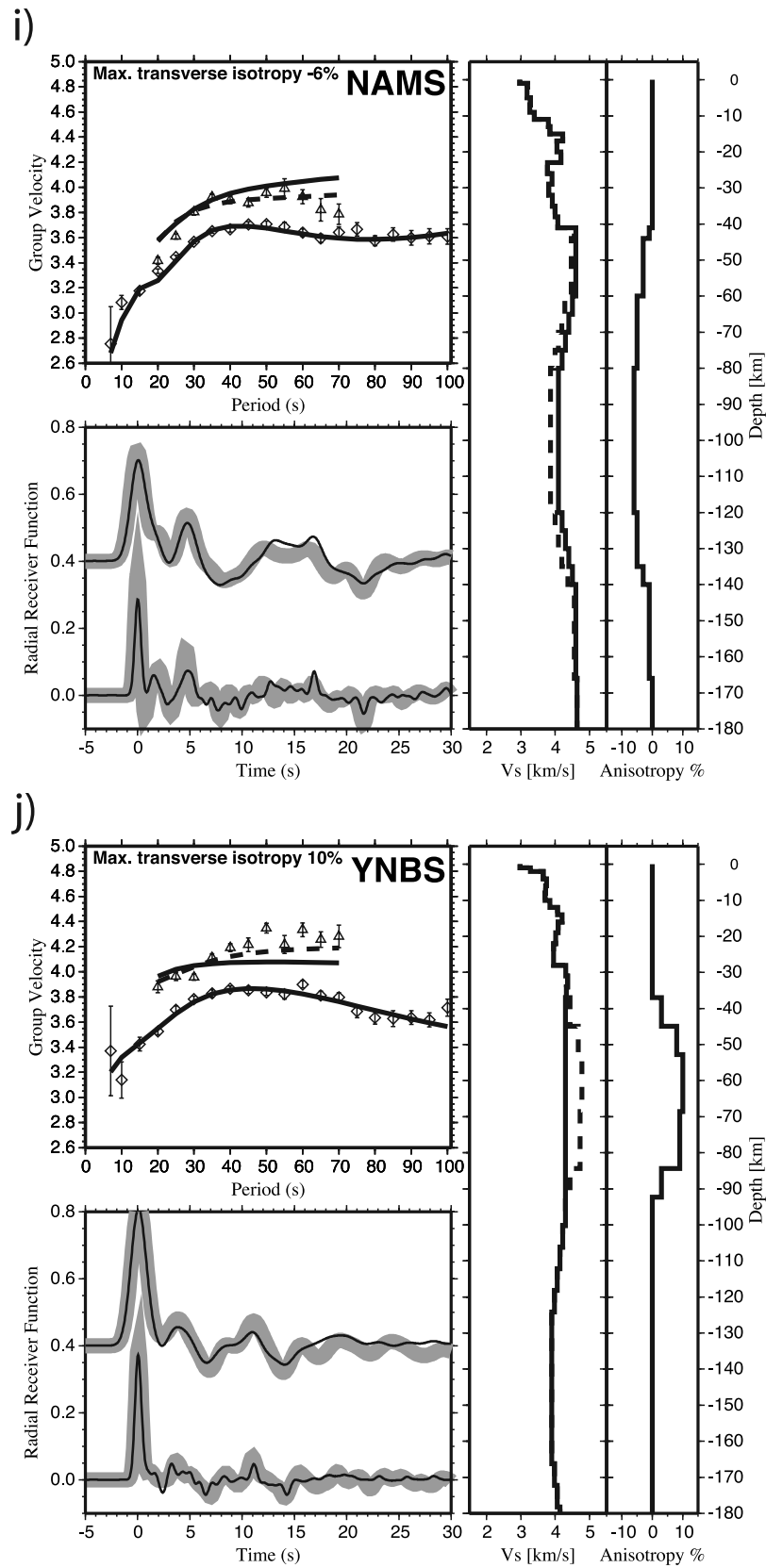


Figure 11. (continued)

of *Al-Damegh et al.* [2005]. We do not observe a prominent lithospheric lid, but instead a low-velocity zone extending from Moho to about 140 km depth, which is very similar to the best model obtained for NAMS. A strong transverse isotropy (about  $-10\%$ ) with  $v_{SV} > v_{SH}$  is required in order to explain Love-Rayleigh group velocity dispersion discrepancy. In fact, some anisotropy in the crust could also be required, in order to further improve the surface wave dispersion data.

[40] Station HASS (Figure 11d) is characterized by 4-km-thick sediments, which is consistent with the results of *Mooney et al.* [1985] and the model CRUST 2.0 (G. Laske, CRUST 2.0, A New Global Crustal Model at  $2^\circ \times 2^\circ$ , 2000, <http://mahi.ucsd.edu/Gabi/crust2.html>, hereinafter referred to as Laske, unpublished report, 2000). However, this is half that determined by *Al-Damegh et al.* [2005]. We explain the difference by our additional constraints from surface wave group velocities. The Moho appears to be gradational, but the crustal thickness does not exceed 40 km, which is consistent with  $v_p/v_s$  analysis and inconsistent with a grid search analysis for receiver functions fits only, presented by *Al-Damegh et al.* [2005]. Again, we believe that surface wave dispersion data provide critical constraints when estimating lithospheric structure. Moreover, the best model for station HASS contains a thick high-velocity lithospheric lid (down to about 120 km) and a low-velocity zone beneath it. A strong transverse isotropy (with  $v_{SH} > v_{SV}$  up to  $8\%$ ) coinciding with the mantle lid is required in order to explain jointly receiver functions and Rayleigh and Love wave group velocities.

[41] Station HILS (Figure 11e) data are the best example of data that do not require a complex lithospheric structure to explain all of the data. The data from this station were also characterized as the best data used in the study of *Al-Damegh et al.* [2005]. We obtain crustal thickness of 35–38 km, a very similar value as in that study, and a relatively good fit for a grid search inversion with only three layers in the crust and one layer below the crust (Figures 6, 7, 8a and 8b). Somewhat controversial, however, is a low velocity obtained for 1-km-thick surface layer, presumably representing sediments and/or a weathered surface layer. This low velocity is partially a result from the observed slow Rayleigh wave group velocity at very short periods (Figure 7b). This is in agreement with the model by *Rodgers et al.* [1999], but it does not agree with the crustal model CRUST2.0 by Laske (unpublished report, 2000) (for a discussion, see *Tkalčić and Laske* [2003]). The velocity contrast at the Moho is not very large (Figure 12) and Moho appears rather gradational. It does not appear that the lithospheric lid and LVZ are strongly pronounced features in the mantle under HILS. The shear velocity in the mantle is comparable with that of nearby station ARSS.

[42] The station HITJC (Figure 11f) is located in southern Jordan, in the northwestern part of the Arabian Peninsula. Our best model contains 2 km of sediments ( $v_s$  varying from 1.85 in the first to 2.51 km/s in the second kilometer), and an additional 1-km-thick layer of arguably slow shear wave velocity (3.07 km/s). This is at least 1 km thicker than reported in CRUST 2.0 (Laske, unpublished report, 2000). The crustal structure is characterized by a midcrustal discontinuity at 15 km depth, with  $v_s$  increasing from 3.52 to 3.8 km/s. We estimate gradational Moho between 33 and

36 km. This is consistent with crustal thickness figure reported by *Al-Damegh et al.* [2005] for stations HITJ and JMOS. In order to simultaneously fit RFs and SWGV dispersion curves, we obtain a lithospheric lid extending to 90 km depth, characterized by high values of horizontally polarized shear waves (and transverse isotropy of  $10\%$ ) and a LVZ with minimum shear velocity of 4 km/s. This is consistent with the results for two stations in the eastern Arabian Shield (KBRS and YNBS. For a comparison, see Figure 12.

[43] Station KBRS (Figure 11g) is an example of a station which has a simple crustal but a complex mantle structure resulting in models that cannot fit jointly the observed receiver functions and both Love and Rayleigh surface wave group velocity dispersion curves. A gradational Moho between 35 and 38 km is featured in our best model. The data for this station had to be modeled by introducing a thin lithospheric lid and a low-velocity zone in the upper mantle in order to match low velocities observed in the group velocity dispersion at intermediate periods (40 to 70 s). A strong transverse isotropy (with  $v_{SH} > v_{SV}$  slightly above  $10\%$ ) is required in the upper mantle extending from Moho down to about 70 km in order to fit longer periods of Love wave group velocity dispersion. Some anisotropy ( $v_{SH} > v_{SV} \sim 3\%$ ) in the lowermost crust is also required in order to explain high velocities at shorter periods of Love wave group velocity dispersion. While transverse isotropy is opposite in sign from that observed at BLJS and NAMS in the southeastern part of the Arabian Peninsula, it is in agreement (both in terms of sign and amplitude) with transverse isotropy obtained for neighboring station YNBS and Jordanian station HITJC.

[44] Station MEZE (Figure 11h) is characterized by a very small number of useful receiver function data. This is partially due to the fact that it operated for only about 10 months with various instrumentation problems. Our averaged receiver function is thus based only on five receiver functions that were consistent enough to be stacked and averaged. It is the noisiest receiver function analyzed in this study and the most difficult to deal with. Therefore we present only a simple grid search results (step 1) in combination with forward modeling (step 4). We obtain slightly smaller crustal thickness than at HASS (about  $38 \pm 2$  km), with overall crustal velocities very comparable to HASS models, however, without recognizable sediments. We cannot expect to entirely infer sediment thickness from only step 1; however, the shape of Rayleigh wave dispersion curve is very similar to HASS. Love wave velocities are slower than for HASS. Thus, unlike in the modeling for HASS, it does not appear that any transverse isotropy in the mantle is needed to explain jointly Love and Rayleigh wave group velocities (see Figures 11h and 11d).

[45] For station NAMS (Figure 11i), the process of fitting the data admittedly proved more challenging than for most of the stations, and as a result RFs for  $a = 1.0$  are not as well fit between 10 and 20 s. From our best model, midcrustal structure is characterized by a transition from slow to fast shear wave speeds (exceeding 4 km/s) and a sudden drop of speeds at about 23 km depth by 0.6 km/s. A significant midcrustal discontinuity ( $v_s$  jumps from 3.39 to 3.8 km/s) and the crustal thickness estimates of 41 km in our best model are in agreement with those of *Al-Damegh et al.* [2005]. We observe somewhat a strong contrast in the shear

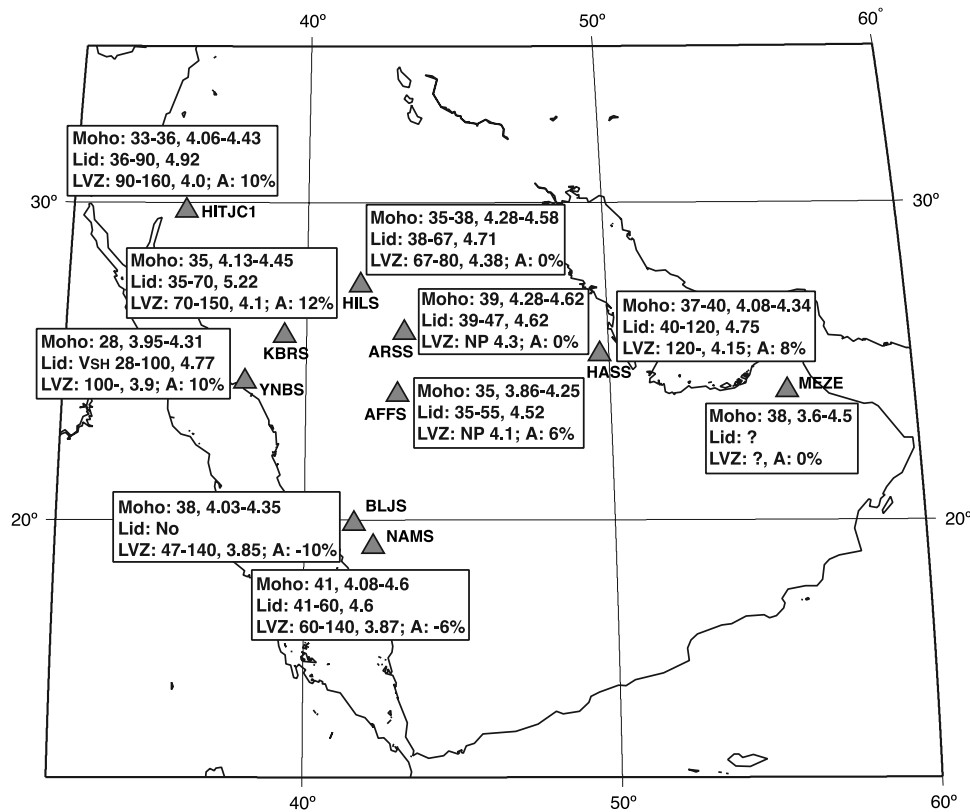


**Figure 12.** Map of station locations (triangles) and the values estimated in the modeling presented in Figures 11a–11e. Line 1 is Moho depth, shear wave velocity values in the layer above and the layer below Moho; line 2 is lithospheric lid thickness, maximum shear wave velocity in the lid ( $v_{SV}$  or  $v_{SH}$ ); line 3 is thickness of the low-velocity zone (NP, not pronounced), minimum shear wave velocity in the LVZ ( $v_{SV}$  or  $v_{SH}$ ); maximum percentage of  $v_{SH} > v_{SV}$  transverse isotropy.

velocity at Moho. The lithospheric lid of only about 20 km thickness, overlaying a broad low-velocity zone that extends to about 140 km depth, is a well-pronounced feature in the upper mantle, because a low-velocity zone beneath it is well pronounced as well. In order to jointly fit Rayleigh and Love wave dispersion, a broad transverse isotropy coinciding with the low-velocity zone in the mantle is required, with  $v_{SV}$  exceeding  $v_{SH}$  by 6%. The sign of transverse isotropy is the same as for BLJS, located just 100 km to the northwest and opposite from the stations located in the northern part of the Red Sea.

[46] Station YBNS (Figure 11j) lies in the northern part of the Red Sea coast. The closest analyzed station in this study is station KBRs, for which we found a strong transverse isotropy. YBNS is a station with considerably thinner crust (28 km) than modeled in this study for other stations, which is consistent with previous study of *Al-Damegh et al.* [2005]. Interestingly, CRUST 2.0 (Laske, unpublished report, 2000) reports four different crustal thickness values in the proximity of this station, ranging from 15 to 40 km, indicating that YBNS is situated in the region with strong lateral gradients in crustal properties. The mantle velocity is low (4.2 km/s on average), and only if we consider fast  $v_{SH}$ , a lithospheric lid is visible in the final model. However, the overall shear wave velocity in the mantle is very low, as expected from the station's vicinity to Red Sea spreading. The data and the final models between YBNS and KBRs

look very similar in that they both require the existence of slow lithospheric mantle and a strong transverse isotropy. For YBNS, our best model has 3.9 km/s minimum shear velocity in LVZ and 8% transverse isotropy, with  $v_{SH} > v_{SV}$  (Figure 12). The sign of transverse isotropy is the same as that obtained for KBRs and HITJC, and opposite from the sign modeled for stations NAMS and BLJS, located in the southwestern part of the Arabian Shield.

## 5. Discussion and Conclusions

[47] In this study we applied a new method involving a combination of grid search, iterative inversions and forward modeling to simultaneously explain the SWGV dispersion (from 7 to 100 s for Rayleigh and 20 to 70 s for Love waves) and teleseismic RF observations at the broadband stations installed on the Arabian Peninsula. For the grid search we used a database of precalculated theoretical receiver functions and dispersion curves, which allowed us to significantly reduce the computational time and investigate a wide range of structural models. We initially fit receiver functions and shorter-period dispersion curves with the structure within the crust and immediately beneath the crust. We then used an additional grid search to characterize the lithospheric lid and low-velocity zone in the upper mantle, fixing the crustal structure and fitting longer-period dispersion curves. Finally, when needed, we forward modeled the transverse isotropy to

simultaneously fit Love and Rayleigh group velocity dispersion. The method proved to be robust and could be in the future applied in the cases where a little a priori knowledge exists about the crustal structure. Additionally, as a result of the “step by step” approach to recover the structure starting from the “top” and ending with the “bottom” of the model, the multistep method MSA4 revealed that the both velocity and transverse isotropy variations in the upper mantle under the Arabian Peninsula are needed to simultaneously fit all data.

[48] Crustal thicknesses that we obtain using MSA4 method generally agree well with those obtained by *Al-Damegh et al.* [2005], who used only receiver functions to constrain the seismological structure of the Arabian Peninsula. This is not surprising because receiver functions are sensitive to strong velocity gradients in the crust and mantle. However, at least in one case (station AFFS), we infer different crustal and sediment thicknesses from those presented by *Al-Damegh et al.* [2005]. We obtained crust as thin as 26 km beneath YNBS, a station located on the coast of the Red Sea (while neighboring KBRS station to the northeast has 36 km thick crust), and maximum crustal thickness of 41 km for station NAMS in the southwestern part of the Arabian Shield along the 2 km escarpment. This agrees with previous studies, which found rapid crustal thinning toward the Red Sea [e.g., *Mooney et al.*, 1985; *Sandvol et al.*, 1998b; *Kumar et al.*, 2002; *Al-Damegh et al.*, 2005]. We did not find strong evidence for crustal thickening toward the Arabian Platform. The crust is between 35 and 40 km thick across the shield, and there is no simple correlation with the eastward distance from the Red Sea for the stations we analyzed (see Figure 12). This lack of variability in Moho depths is consistent with CRUST 2.0 model (Laske, unpublished report, 2000), although the depths we obtain are on average about 5 km shallower than in CRUST 2.0. In the Arabian Platform, we obtain 40 km thick crust beneath station HASS. Although the data quality for station MEZE is poor, the estimated crustal thickness of 38 km beneath that station is similar to that beneath HASS. *Al-Amri and Gharib* [2000] reported 45 km thick crust under RIYD station, approximately halfway between AFFS and HASS. Recently, *Pasyanos et al.* (submitted manuscript, 2005) reported 45 km thick crust under Kuwait. These variable results suggest that the crustal thickness in the Arabian Platform perhaps varies laterally by as much as 5–10 km. Indeed, frequency histograms of binned observed Love and Rayleigh wave group and phase velocities as well as histograms of binned crustal thicknesses for the Arabian Platform do not follow simple normal distribution and indicate a significant level of crustal complexity [*Laske and Tkalčić*, 2002; *Tkalčić and Laske*, 2003]. Thus the crustal thickness of the Arabian Platform remains somewhat controversial, and clearly more stations and more data are needed to resolve this uncertainty. Unfortunately, there are very few hard rock outcrops for broadband deployments in the platform.

[49] We think that the SWGV data combined with RFs improve previous velocity models, particularly absolute values of velocity at all depths. We found 4 km of sediments beneath the station HASS in the Arabian Platform and 2 km of sediments for station HITJC in Jordan. We also found 1-km-thick layer of low velocity at HILS, which is consistent with results of *Rodgers et al.* [1999] and incon-

sistent with CRUST 2.0 (Laske, unpublished report, 2000). The extreme values of upper mantle shear velocities range from very low 3.85 km/s in LVZs (BLJS and NAMS) to very high 5.2 km/s (KBRS) in lithospheric lids. We observe a very thin lithospheric lid at two stations in the southwestern part of the Arabian Shield (BLJS and NAMS), as well as in the eastern part of the shield (HILS, ARSS and AFFS). This observation is consistent with findings of *Julià et al.* [2003] although they studied data from different stations. Very low shear wave velocities across the shield are consistent with anomalously hot upper mantle, which might be a consequence of a broad lateral thermal anomaly extending from east Africa [e.g., *Nyblade et al.*, 2000; *Romanowicz and Gung*, 2002; *Benoit et al.*, 2003].

[50] We infer some strikingly high values of polarization anisotropy in the mantle and sometimes in the lower crust, as well as prominent lateral variations in the direction of fast polarization axis ( $v_{SV} > v_{SH}$  in the southwestern part of the Arabian Peninsula and  $v_{SH} > v_{SV}$  for the rest of the stations where transverse isotropy was obtained). Because the parameterizations of anisotropy are different, it is difficult to compare our result with a study of SKS splitting [*Wolfe et al.*, 1999], which finds uniform north-south orientation of fast polarization axis in horizontal plane and the delay time between fast and slow shear waves from 0.5 to 1.5 s. In tectonically active regions like the Arabian Shield, the upper mantle is most likely stratified with varying values of anisotropy in the both amplitude and direction [e.g., *Christensen et al.*, 2001] and this can complicate interpretation of SKS splitting. Although propagation anisotropy in the mantle averages 4% [*Smith and Ekström*, 1999], individual hand samples of mantle xenolites show significantly higher anisotropy [e.g., *Christensen et al.*, 2001; *Meltzer and Christensen*, 2001; *Christensen*, 2002]. This is expected because anisotropy strength measured from seismic waves averages over large volumes of mantle rocks. One interpretation of laterally varying transverse isotropy in our models is that the relationship between strain field and lattice preferred orientation of minerals also varies laterally. Interestingly, in the southwestern part of the Arabian Shield, in the vicinity of the Red Sea, the lithosphere appears to be thinned beneath stations BLJS and NAMS, where we observe fast polarization oriented along vertical axis. In contrast, in the northwestern part of the Arabian Shield, we obtain fast polarization axis in the horizontal plane with relatively thick lithosphere. Such strong lateral variations are also seen in recent attenuation maps of Sn and Pn waves for the Red Sea region [*Al-Damegh et al.*, 2004]. These observations strongly suggest that the Red Sea spreading, as well as the mantle flow pattern, is probably not uniform along the axis of the Red Sea.

[51] **Acknowledgments.** We thank J. Julià and C. J. Ammon for making their iterative inversion code available. We thank A. Levshin and two anonymous reviewers for their constructive comments, which helped greatly in improving the manuscript. This work was performed under the auspices of the U.S. Department of Energy by University of California, Lawrence Livermore National Laboratory, under contract W-7405-Eng-48. This is LLNL contribution UCRL-JRNL-216666.

## References

Al-Amri, A. M. (1999), The crustal and upper-mantle structure of the interior Arabian platform, *Geophys. J. Int.*, 136, 421–430.

- Al-Amri, A. M., and A. A. Gharib (2000), Lithospheric seismic structure of the eastern region of the Arabian Peninsula, *J. Geodyn.*, *29*, 125–139.
- Al-Amri, M. S., and A. M. Al-Amri (1999), Configuration of the Seismographic networks in Saudi Arabia, *Seismol. Res. Lett.*, *70*, 322–331.
- Al-Damegh, K., E. Sandvol, A. Al-Lazki, and M. Barazangi (2004), Regional seismic wave propagation (Lg and Sn) and Pn attenuation in the Arabian Plate and surrounding regions, *Geophys. J. Int.*, *157*, 775–795.
- Al-Damegh, K., E. Sandvol, and M. Barazangi (2005), Crustal structure of the Arabic plate: New constraints from the analysis of teleseismic receiver functions, *Earth Planet. Sci. Lett.*, *231*, 177–196.
- Ammon, C. J. (1991), The isolation of receiver effects from teleseismic P waveforms, *Bull. Seismol. Soc. Am.*, *81*, 2504–2510.
- Ammon, C. J., G. E. Randall, and G. Zandt (1990), On the non-uniqueness of receiver function inversions, *J. Geophys. Res.*, *95*, 15,303–15,318.
- Anderson, D. L. (1961), Elastic wave propagation in layered anisotropic media, *J. Geophys. Res.*, *66*, 2953–2963.
- Benoit, M., A. Nyblade, J. vanDecar, and H. Gurrrola (2003), Upper mantle P wave velocity structure and transition zone thickness beneath the Arabian shield, *Geophys. Res. Lett.*, *30*(10), 1531, doi:10.1029/2002GL016436.
- Birch, F. (1961), The velocity of compressional waves in rocks to 10 kilobars, part 2, *J. Geophys. Res.*, *66*, 2199–2224.
- Camp, V., and M. Roobol (1992), Upwelling asthenosphere beneath western Arabia and its regional implications, *J. Geophys. Res.*, *97*, 15,255–15,271.
- Christensen, N. I. (2002), Continental mantle seismic anisotropy: A new look at the Twin Sisters massif, *Tectonophysics*, *355*, 163–170.
- Christensen, N. I., L. G. Medaris Jr., and H. F. Wang (2001), Depth variation of seismic anisotropy and petrology in central European lithosphere: A tectonothermal synthesis from spinel lherzolite, *J. Geophys. Res.*, *106*, 645–664.
- Du, Z. J., and G. R. Foulger (1999), The crustal structure beneath the northwest fjords, Iceland, from receiver functions and surface waves, *Geophys. J. Int.*, *139*, 419–432.
- Dziewonski, A. M., and D. L. Anderson (1981), Preliminary reference Earth model, *Phys. Earth Planet. Inter.*, *25*, 297–356.
- Gaherty, J. B. (2004), A surface wave analysis of seismic anisotropy beneath eastern North America, *Geophys. J. Int.*, *158*, 1053–1066.
- Gaherty, J. B., and T. H. Jordan (1995), Lehmann discontinuity as the base of an anisotropic layer beneath continents, *Science*, *268*, 1468–1471.
- Hansen, S. E., S. Y. Schwartz, A. J. Rodgers, and A. Al-Amri (2006), Combined plate motion and density driven flow in the asthenosphere beneath Saudi Arabia: Evidence from shear-wave splitting and seismic anisotropy, *Geology*, *34*, 869–872.
- Julià, J., C. J. Ammon, R. B. Herrmann, and A. M. Correig (2000), Joint inversion of receiver function and surface wave dispersion observations, *Geophys. J. Int.*, *143*, 1–19.
- Julià, J., C. J. Ammon, and R. B. Herrmann (2003), Lithospheric structure of the Arabian Shield from the joint inversion of receiver functions and surface wave dispersion, *Tectonophysics*, *371*, 1–21.
- Kennett, B. L. N. (1983), Approximations to the response of the stratification, in *Seismic Wave Propagation in Stratified Media*, chapter 9, Cambridge Univ. Press, New York.
- Knopoff, L., and A. A. Fouda (1975), Upper mantle structure under the Arabian Peninsula, *Tectonophysics*, *26*, 121–134.
- Kumar, M. R., D. S. Ramesh, J. Saul, D. Sarkar, and R. Kind (2002), Crustal structure and upper mantle stratigraphy of the Arabian shield, *Geophys. Res. Lett.*, *29*(8), 1242, doi:10.1029/2001GL014530.
- Langston, C. A. (1979), Structure under Mount Rainier, Washington, inferred from teleseismic body waves, *J. Geophys. Res.*, *84*, 4749–4762.
- Laske, G., and H. Tkalčić (2002), An evaluation of the SAIC regionalized model (part I: Sediment and crustal thicknesses), *Report for SAIC*, 37 pp., Dep. of Energy, Washington, D. C.
- Levin, V., and J. Park (2000), Shear zones in the Proterozoic lithosphere of the Arabian Shield and the nature of the Hales discontinuity, *Tectonophysics*, *323*, 131–148.
- Levin, V., A. Henza, J. Park, and A. Rodgers (2006), Texture of mantle lithosphere along the Dead Sea Rift: Recently imposed or inherited?, *Phys. Earth Planet. Inter.*, *158*, 85–91.
- Ligorria, J. P., and C. J. Ammon (1999), Iterative deconvolution and receiver function estimation, *Bull. Seismol. Soc. Am.*, *89*, 1395–1400.
- Mellors, R. J., F. L. Vernon, V. E. Camp, A. Al-Amri, and A. Ghalib (1999), Regional waveform propagation in the Saudi Arabian peninsula, *J. Geophys. Res.*, *104*, 20,221–20,232.
- Meltzer, A., and N. I. Christensen (2001), Nanga Parbat crustal anisotropy: Implications for interpretation of crustal velocity structure and shear-wave splitting, *Geophys. Res. Lett.*, *28*, 2129–2132.
- Mokhtar, T., and M. Al-Saeed (1994), Shear wave velocity structures of the Arabian Peninsula, *Tectonophysics*, *230*, 105–125.
- Mooney, W. D., M. E. Gettings, H. R. Blank, and J. H. Healy (1985), Saudi Arabian seismic-refraction profile: A traveltimes interpretation of crustal and upper mantle structure, *Tectonophysics*, *111*, 173–246.
- Nyblade, A. A., T. J. Owens, H. Gurrrola, J. Ritsema, and C. R. Langston (2000), Seismic evidence for a deep upper mantle thermal anomaly beneath east Africa, *Geology*, *28*, 599–602.
- Owens, T. J. (1987), Crustal structure of the Adirondacks determined from broadband teleseismic waveform modeling, *J. Geophys. Res.*, *92*, 6391–6401.
- Owens, T. J., S. R. Taylor, and G. Zandt (1987), Crustal structure at regional seismic test network stations determined from inversion of broadband teleseismic P waveforms, *Bull. Seismol. Soc. Am.*, *77*, 631–632.
- Özalaybey, S., M. K. Savage, A. F. Sheehan, J. N. Louie, and J. N. Brune (1997), Shear-wave velocity structure in the northern basin and range province from the combined analysis of receiver functions and surface waves, *Bull. Seismol. Soc. Am.*, *87*, 183–189.
- Pasyanos, M. E. (2005), A variable resolution surface wave dispersion study of Eurasia, North Africa, and surrounding regions, *J. Geophys. Res.*, *110*, B12301, doi:10.1029/2005JB003749.
- Pasyanos, M. E., and W. R. Walter (2002), Crust and upper mantle structure of North Africa, Europe, and the Middle East from the inversion of surface waves, *Geophys. J. Int.*, *149*, 463–481.
- Pasyanos, M. E., W. R. Walter, and S. E. Hazler (2001), A surface wave dispersion study of the Middle East and North Africa for monitoring the Comprehensive Nuclear-Test-Ban Treaty, *Pure Appl. Geophys.*, *158*, 1445–1474.
- Rodgers, A. J., W. Walter, R. Mellors, A. M. S. Al-Amri, and Y. S. Zhang (1999), Lithospheric structure of the Arabian Shield and Platform from complete regional waveform modeling and surface wave group velocities, *Geophys. J. Int.*, *138*, 871–878.
- Rodgers, A. J., D. Harris, S. Ruppert, J. P. Lewis, J. O'Boyle, M. Pasyanos, A. Q. Fandi Abdallah, T. Al-Yazjeen, and A. Al-Gazo (2003a), A broadband seismic deployment in Jordan, *Seismol. Res. Lett.*, *74*, 374–381.
- Rodgers, A. J., P. Lewis, and A. R. Fowler (2003b), A broadband seismic deployment in the United Arab Emirates, *Inf. Doc. UCRL-ID-153713*, 4 pp., Lawrence Livermore Natl. Lab., Livermore, Calif.
- Romanowicz, B., and Y. Gung (2002), Superplumes from the core-mantle boundary to the lithosphere: Implications for heat flux, *Science*, *296*, 513–516.
- Saito, M. (1988), DISPER80: A subroutine package for the calculation of seismic normal-model solutions, in *Seismological Algorithms*, edited by D. J. Doornbos, pp. 294–319, Elsevier, New York.
- Sambridge, M., and G. Drijkoningen (1992), Genetic algorithms in seismic waveform inversion, *Geophys. J. Int.*, *109*, 323–342.
- Sandvol, E., D. Seber, A. Calvert, and M. Barazangi (1998a), Grid search modeling of receiver functions: Implications for crustal structure in the Middle East and North Africa, *J. Geophys. Res.*, *103*, 26,899–26,917.
- Sandvol, E., D. Seber, M. Barazangi, F. R. Vernon, R. Mellors, and A. M. Al-Amri (1998b), Lithospheric seismic velocity discontinuities beneath the Arabian Shield, *Geophys. Res. Lett.*, *25*, 2873–2876.
- Shibutani, T., M. Sambridge, and B. Kennett (1996), Genetic algorithm inversion for receiver functions with application to crust and uppermost mantle structure beneath Eastern Australia, *Geophys. Res. Lett.*, *23*, 1829–1832.
- Silver, P. G. (1996), Seismic anisotropy beneath the continents: Probing the depths of geology, *Annu. Rev. Earth Planet. Sci.*, *24*, 385–432.
- Silver, P. G., and W. W. Chan (1988), Implications for continental structure and evolution from seismic anisotropy, *Nature*, *335*, 34–39.
- Smith, G. P., and G. Ekström (1999), A global study of P<sub>n</sub> anisotropy beneath continents, *J. Geophys. Res.*, *104*, 963–980.
- Tkalčić, H., and G. Laske (2003), An evaluation of the SAIC regionalized model (part II: Comparison of observed with predicted surface wave dispersion), *Report for SAIC*, 96 pp., Dep. of Energy, Washington, D. C.
- Vernon, F. R., and J. Berger (1998), Broadband seismic characterization of the Arabian Shield, final scientific technical report, contract F 19628-95-K-0015, 36 pp., Dep. of Energy, Washington, D. C.
- Vernon, F. R., R. Mellors, J. Berger, A. Edelman, A. Al-Amri, J. Zollweg, and C. Wolfe (1996), Observations from regional and teleseismic earthquakes recorded by a deployment of broadband seismometers in the Saudi Arabian Shield, *Eos Trans. AGU*, *77*, 478.
- Wolfe, C. J., F. R. Vernon III, and A. Al-Amri (1999), Shear-wave splitting across western Saudi Arabia: The pattern of upper mantle anisotropy at a Proterozoic shield, *Geophys. Res. Lett.*, *26*, 779–782.

A. Al-Amri, Geology Department, King Saud University, P.O. Box 2455, Riyadh 11451, Saudi Arabia.

R. Gök, M. E. Pasyanos, A. J. Rodgers, and W. R. Walter, Atmospheric, Earth and Energy Sciences Department, Lawrence Livermore National Laboratory, P.O. Box 808, Livermore, CA 94551, USA.

H. Tkalčić, Multimax, Inc., 5740 Hollis Street, Emeryville, CA 94608, USA. (tkalcic@multimax.com)